AGU PUBLICATIONS

Earth and Space Science

RESEARCH ARTICLE
10.1002/2015EA000119

**Key Points:**
- Fog and low clouds (FLCs) have a significant influence on coastal ecosystem processes
- FLC maps of hourly day and night weather satellite data reveal long-term spatial patterns
- FLC coefficient of variation reveals core areas of interannual stability

**Correspondence to:**
A. Torregrosa,
atorregrosa@usgs.gov

**Citation:**
Torregrosa, A., C. Combs, and J. Peters (2016), GOES-derived fog and low cloud indices for coastal north and central California ecological analyses, *Earth and Space Science*, *3*, doi:10.1002/2015EA000119.

Received 5 JUN 2015
Accepted 11 DEC 2015
Accepted article online 17 DEC 2015



# GOES-derived fog and low cloud indices for coastal north and central California ecological analyses

**Alicia Torregrosa[1], Cindy Combs[2], and Jeff Peters[1]**

[1]Western Geographic Science Center, U.S. Geological Survey, Menlo Park, California, USA, [2]Cooperative Institute for Research in the Atmosphere, Colorado State University, Fort Collins, Colorado, USA

**Abstract** Fog and low cloud cover (FLCC) strongly influences the water, energy, and nutrient flux of coastal ecosystems. Easy-to-use FLCC data are needed to quantify the impacts of FLCC on ecosystem dynamics especially during hot and dry Mediterranean climate summers. Monthly, annual, and decadal FLCC digital maps (indices) were derived for June–September 1999–2009 for coastal California, latitude 34.50°N (south of Monterey Bay) to latitude 41.95°N (north of Crescent City) from 26,000 hourly night and day Geostationary Operational Environmental Satellite (GOES) images. Monthly average FLCC ranges from <2 to 18 hours per day (h/d). Average FLCC over the ocean increases from north (9 h/d) to south (14 h/d), whereas on land, FLCC is highest where land juts into the prevailing NW winds and is lowest in the lee of major capes. FLCC advects farthest inland through low-lying NW ocean-facing valleys. At night, average total hours of FLCC are higher more frequently on land than over the ocean. The interannual FLCC coefficient of variation shows long-term geographic stability that is strongly associated with landform position. FLCC hours per day mapped contours, derived from decadal average FLCC, delineate the commonly used term "fog belt" into FLCC zones with increased locational precision. FLCC indices are available for download from the California Landscape Conservation Cooperative Climate Commons website (http://climate.calcommons.org/datasets/summertime-fog). FLCC indices can improve analyses of biogeographic and bioclimatic species distribution models; understanding meteorological mechanisms driving FLCC patterns; solar energy feasibility studies; investigations of ecohydrology, evapotranspiration, and agricultural irrigation demand; and viticulture ripening models.

## 1. Introduction

This study focuses on fog and low clouds (FLCs) of marine origin, the most common cloud type in coastal California during the seasonally arid Mediterranean climate summer months (June–September) [*Palmer*, 1917; *Leipper*, 1994; *Pilié et al*., 1979; *Koračin et al*., 2014; *Torregrosa et al*., 2014]. The product of this study is a suite of FLC indices that simplify a complex phenomenon by providing a spatiotemporally coherent data set of fog and low cloud cover (FLCC). The indices were developed to explore patterns of coastal FLC that arise from interactions of air, ocean, and land surface processes and to quantify FLC as an input for ecological investigations.

### 1.1. Marine Fog in Coastal California

Fog is a category of low cloud that is variously defined by its meteorological formation process, the obstruction it presents to transportation, or its functional contribution to ecosystems. The primary definition of fog is a cloud whose base touches the ground [*Houze*, 2014]. Colloquially, the term fog is used to describe the layer of marine stratus and stratocumulus clouds with base heights of up to 2 km that are commonly perceived by coastal residents to produce a foggy summer morning. The *American Meteorological Society* [2014] and *Federal Aviation Administration* [2013] define fog as suspended water droplets close to the Earth that reduce visibility below 1 km (0.62 miles).

The dominant summer cloud pattern is driven by an eastern North Pacific high-pressure system (High) formed by the warm and dry descending branch of the Hadley cell. The subsiding air mass of the High caps the marine atmospheric boundary layer (MABL), a layer of air close to and strongly influenced by the cold Pacific Ocean surface and the periodically colder oceanic currents upwelled to the ocean surface by northwest winds [*García-Reyes and Largier*, 2012]. Within the MABL, water vapor in the buoyant ascending air masses gets cooled by expansion and condenses on salts from sea spray and other suspended aerosols to form an expansive marine stratus cloud that can, at times, convect into a multitude of individual

stratocumulus clouds [*Wood*, 2012]. The vertical thickness of the low cloud layer remains relatively constant as dissolution and formation processes balance each other out. The cloud loses thickness when moist air at the top becomes entrained into the warmer, drier air aloft. The cloud gains thickness from below when buoyant moist air near the ocean surface rises to its "lifted condensation level" replenishing the condensed droplets lost at the cloud top. Buoyancy and land surface heating lifts the cloud away from the Earth's surface, but the upper air inversion acts to keep it lowered. The low cloud layer will dissipate with sufficient turbulence, wind shear, and cloud top radiative cooling [*Lilly*, 1968; *Lester*, 1985; *Wood and Bretherton*, 2006; *Pruppacher and Klett*, 2010; *Wood*, 2012; *Houze*, 2014].

A strong coastal to inland temperature gradient forms when the land surface heats or cools. The gradient drives both offshore and onshore breezes that advect the marine layer across the landscape. The coastal mountains add terrain complexity to the air-ocean-land system [*Dorman et al*., 2013]. The variations in elevation and slope steepness, low-lying gaps that funnel winds, and differential heating of north versus south facing slopes modify the temperature and pressure gradients that form, move, and dissipate FLC [*Terjung et al*., 1969; *Filonczuk et al*., 1995; *Koračin et al*., 2005, 2014; *Taylor et al*., 2008; *Nicholson*, 2011].

Many unknowns remain about the details of FLC formation and dissipation. As a result, FLC continues to be difficult to forecast on both long and short time scales [*Kann et al*., 2015]. Daily and diurnal patterns are chaotic, turbulent, and, because of the importance to air traffic, well recorded. From these records, strong correlations show up between the formation and transport of FLC and the strength of seasonal drivers that fluctuate in concert with global atmospheric and oceanic cycles [*Trenberth and Hurrell*, 1994; *García-Reyes and Largier*, 2012; *Seo et al*., 2012; *Johnstone and Mantua*, 2014; *Redmond and Abatzoglou*, 2014; *Schwartz et al*., 2014]. Airport FLC records have been very useful as primary sources for air quality and ecological research [*Beer and Leopold*, 1947; *LaDochy and Witiw*, 2012; *Johnstone and Dawson*, 2010; *Williams et al*., 2015]; however, these are point data and insufficient to answer many spatial ecological questions by themselves. The temporally and spatially continuous grid format of the data set described in this study offers an alternative analytic approach.

### 1.2. Clouds and Coastal Ecosystems

Clouds cycle water and alter the incoming and outgoing flux of energy thereby regulating ecosystem dynamics at local to global scales [*Wielicki et al*., 1996; *Trenberth et al*., 2009]. In coastal California FLC adds water and lowers temperatures during the hot and dry Mediterranean climate summer affecting the pattern of species distribution across the landscape [*Leipper*, 1994; *Gilliam*, 2002; *Azevedo and Morgan*, 1974; *Hiatt et al*., 2012; *Iacobellis and Cayan*, 2013]. As a consequence FLC is a key feature of coastal ecosystem and has numerous and strong impacts on ecological processes [*Weathers*, 1999; *Mooney et al*., 2001].

Increased relative humidity from FLC and lowered temperatures from blocked shortwave radiation reduce plant evapotranspiration stress [*Fischer et al*., 2009; *Baguskas et al*., 2014]. Fog water droplets coalesce on surfaces such as pine needles, fern fronds, and spider webs accumulating and dripping into the soil adding occult precipitation to shallow root systems [*Katata et al*., 2010; *Valiente et al*., 2011] and increasing below-ground microbial community productivity [*Carbone et al*., 2013]. Fog drip also increases streamflow [*Gurnell*, 1976; *Harr*, 1982]. During extreme late summer low streamflow conditions, fog events can result in sufficient fog drip and reduced evapotranspiration to increase streamflow by 200% [*Sawaske and Freyberg*, 2014]. Plants capable of direct water uptake into internal tissues from their leaf or bark surfaces benefit to varying degrees from fog events [*Slatyer*, 1960; *Dawson*, 1998; *Limm et al*., 2009; *Earles et al*., 2015].

In addition to direct water, nutrient, and particulate inputs [*Gundel et al*., 1994; *Weathers et al*., 2000; *Collett et al*., 2002; *Herckes et al*., 2013], FLCC also has cascading ecosystem benefits. Reduced net radiation lowers stream temperature during critical times of low streamflows, benefitting salmonids and other fish species that require cool stream temperatures [*Madej et al*., 2006; *Madej*, 2010]. Frequent FLCC reduces the likelihood of forest fires [*Norman et al*., 2009] and extreme heat events [*Iacobellis and Cayan*, 2013], the latter correlated with increased instances of emergency medical requests from vulnerable human populations [*Gershunov and Johnston*, 2011]. Summer heat waves, such as those that occurred during the relatively FLCC-free month of July 2006, increased the risk of mortalities in all ecosystem populations, from human [*Knowlton et al*., 2009] to intertidal invertebrates [*Helmuth et al*., 2007]. Marine life is at increased risk of catastrophic die-off when summer low tides coincide with cloud-free summer days [*Mislan et al*., 2009]. FLCC intensifies coastal-to-inland oceanity gradients of temperature and moisture [*Mass et al*., 1986; *Bailey*, 2009]. The combination of steep oceanity gradients and

complex coastal terrain increases bioclimatic diversity [*Torregrosa et al*., 2013]. All these effects have landscape-level impacts on vegetation patterns, species distribution, species refugia, carbon sequestration, agricultural irrigation demand, and urban energy use [*Borthagaray et al*., 2010; *Baguskas et al*., 2014; *Barbour et al*., 2014; *Vasey et al*., 2014].

The inland incursion of the marine stratus and stratocumulus layer has a long history as an explanatory factor for coastal vegetation distribution patterns. By the turn of the last century, the term fog belt was described as "well known" in scientific literature [*Cannon*, 1901] and a factor for coastal redwood distribution but with no precise definition. The term fog belt has continued to be used without being well defined [*Shreve*, 1927; *California Department of Water Resources*, 2012].

Higher-resolution maps that can better define the spatial and temporal variability of FLCC will improve our understanding of landscape-level ecosystem dynamics of coastal California systems; however, generating these maps is challenging. FLCC is extremely variable affecting ecosystem processes through different pathways. FLCC varies in duration sometimes lasting for days or disappearing within minutes. FLCC varies spatially with a horizontal range of 0 to 5000 km wide, vertical thickness range of tens to hundreds of meters (m), and a cloud base at 0 to 2000 m from the Earth's surface. FLCC varies in droplet density and chemical composition. Further complicating FLCC-related landscape-level mapping and analysis is the voluminous amount of data, "big data," that are needed to capture ecologically relevant patterns. The goal of this study is to provide FLCC indices that compress large quantities of data into manageable units that are useful for landscape-level analysis.

### 1.3. Satellite-Derived Fog and Low Cloud Frequency

Many satellite sensors have been used to investigate FLC. Sensors on satellite platforms that move in a Sun-synchronous orbit such as the Moderate Resolution Imaging Spectroradiometer (MODIS) and the advanced very high resolution radiometer (AVHRR) provide views of FLC once or twice daily and have been used to investigate annual and decadal FLC variability [*Platnick et al*., 2003; *Bendix et al*., 2006; *Jensen et al*., 2008] The National Oceanic and Atmospheric Administration (NOAA) Geostationary Operational Environmental Satellite (GOES) maintains a "stationary" Earth view and provides continuous imagery every 15 or 30 minutes, day and night. An impressive effort to evaluate locations for fog water harvesting in Chile by *Cereceda et al*. [2003] classified pixels for 11,000 daytime GOES images from May 2001 to April 2003 as either clear sky or cloud to generate fog probability data. That study was an early inspiration for this work.

Most cloud mapping, including all the examples in the previous paragraph, uses data from the visible light channel (constrained to daytime). Shortwave and thermal infrared channels can also be used to classify pixels as clear sky or cloud at night. Low stratus/stratocumulus and high cirrus clouds have nearly opposite thermal properties that can be used to differentiate pixels of fog and low cloud (FLC) from high clouds [*Ellrod*, 1995; *Jedlovec et al*., 2008; *Jedlovec*, 2009]. Cirrus is a high, cold, and wispy cloud that is relatively transparent to shortwave radiation with low albedo. Stratus and stratocumulus are lower, warmer clouds with more water vapor and liquid droplets that strongly reflect shortwave radiation (high albedo). Both are effective at absorbing outgoing longwave radiation [*Chen et al*., 2000].

Classifying pixels in an image based on differences in thermal properties is computationally demanding due to the need to include in the computation the high temporal and spatial variability of the underlying land surface temperature [*Lee et al*., 1997; *Jedlovec*, 2009]. The absolute temperature difference between low clouds and the Earth's surface changes as the Earth's surface temperature changes. Both the Earth's surface and the cloud temperatures are continuously changing during the day because they are receiving, reflecting, and, based on their temperature and composition, reemitting differing amounts of solar radiation. Throughout the day and night, clouds can absorb and reemit the infrared radiation reemitted from the land or ocean surface. In addition, the land surface is not homogeneous. Each land surface cover type has a different emissivity at the same temperature. Interannual, seasonal, and diurnal differences in solar radiation received at the surface add additional thermal variation. For cloud mapping this means that accurate classification of pixels into low, high, and no cloud categories requires changing temporal and spatial baselines, as is done in this study.

The NOAA Comprehensive Large Array-Data Stewardship System (CLASS) archive is a rich source of raw and derived satellite data and products; however, the data are not easy to process without atmospheric science

**Table 1.** Ecological Questions Driving the Development of FLCC Indices

| Question | FLCC Index |
|---|---|
| Are fog and low cloud cover (FLCC) frequency patterns and plant species distribution correlated? If so, for which species and how strongly? | Percent FLCC over the regeneration period of the vegetation in question (years to decades) |
| What is the relative impact of FLCC on maximum stream and air temperatures? Can a generalized climatological relationship be extracted for use in future climate modeling and historical reconstructions? | Percent FLCC on a daily, monthly, annual, and decadal interval |
| Does FLCC affect late summer climatic water deficit? | Cumulative summer season FLCC and end-of-season (September) FLCC |
| How much does FLCC alter incident solar radiation (total intensity, direct, and diffuse)? How much does the FLCC-reduced radiation affect evaportranspiration? Does nighttime fog drip impact evapotranspiration? | FLCC daytime versus nighttime periods (daily, monthly, seasonal, and decadal) |
| How much does FLCC impact watershed hydrological variations measured against stream gage flow? | FLCC at intervals corresponding to stream gage data (diurnal, daily, monthly, and summer cumulative) |

software platforms such as the Man Computer Interactive Data Access System (McIDAS) [*Santek et al*., 2006]. Nonetheless, GOES data are being used increasingly for more than their original purpose of real-time weather forecasting. *Iacobellis and Cayan* [2013] derived daytime GOES cloud reflectivity (cloud albedo) as a proxy for cloudiness and, in conjunction with radiosonde-derived vertical environment profiles, found inversion base height to be a key driver of inland FLC incursion.

Near-real-time FLC products are made available for aviation and weather forecasting purposes, but long-term archived data suitable for historical analysis of interactions between coastal fog and ecological systems are not. As a result, the natural resource management community of north and central California still lacks quantitative assessments of fog frequency and distribution suitable for ecological analysis. The data products produced by this study use archived night and day GOES imagery, with high temporal frequency, to produce indices relevant to both diurnal and nocturnal processes and suited to investigate ecological impacts associated with variations in FLC.

### 1.4. FLCC Indices for Ecological Application

As previously described, FLCC impacts coastal ecosystems by modifying the basic constituents of ecosystem processes: water and energy. This suggests that improved quantification of FLCC is relevant to a potentially wide and overwhelming range of ecological applications, from empirical and fundamental biogeographical questions about FLCC thresholds associated with geographic distributions of coastal species to mechanistically based predictions about how changes in an FLCC regime impact ecological function.

Many different indices could be extracted from satellite data to describe key FLC and FLCC parameters to facilitate ecological analyses. Understanding FLCC-related processes with distinct temporal mechanisms requires that FLCC data sets be extracted into indices for those relevant time periods. To make the study more tractable, a set of key ecological questions (Table 1) were identified by an interdisciplinary group of land managers and scientists during the April 2012 Pacific Coastal Fog Workshop, Menlo Park, California (see http://geography.wr.usgs.gov/fog/archives.html). The questions were used as a starting point to identify specific temporal intervals of FLCC variability that would be ecologically relevant and the specific type of information to be contained within the index for that time interval.

Questions related to broad distributional patterns such as "what are the FLCC thresholds associated with landscape patterns of maritime chaparral, redwood forest, and other coastal California natural communities?" could be addressed with maps of FLCC patterns from a decadal time frame. Questions that are associated with radiation budgets such as "what is the relative impact of FLCC on stream temperatures?" or those related to evapotranspiration would require FLCC indices for both the daytime period of direct solar irradiance and the nighttime period of reemitted infrared. In the Mediterranean climate landscape a strong indicator of relative impact on plant growth is the climatic water deficit (CWD) during September, usually the hottest and driest time of the year. Two time periods that would contribute to investigations of the impact of FLCC on CWD are cumulative summer season FLCC and September FLCC. The latter would help assess how much FLCC attenuates the arid conditions at the end of the summer season.

In addition to the challenge of defining time intervals for indices is the challenge of defining the unit of analysis for the indices. Table 1 lists several different units associated with different questions. For example,

questions relevant to broad decadal patterns list percent cover as the unit of analysis, whereas questions regarding CWD require cumulative hours of FLCC over the entire specified time interval. For this study we use "hours per day" (h/d) as the unit of analysis. This measure is similar to percent cover in that it provides a relative percentage of cover; however, rather than a base of 100, it uses a base of 24 h. Either measure could be used; however, our use of h/d is intended to facilitate an intuitive grasp of the amount of FLCC affecting the ecological process of interest on a daily time step.

The indices are intended to repurpose FLCC data into an easy-to-use format that can be added directly into models, algorithms, or digital maps. The indices represent an important climate variable that can be used to help answer questions about the impact of FLCC on coastal ecosystems in both wild and urbanized settings.

## 2. Methods

The geographic study area is the California coast from latitude 34.50°N, Point Arguello, Santa Barbara County, to latitude 41.95°N, north of Crescent City, Del Norte County. The study focuses on the dry season defined as June–September when the impact from FLCC is greatest and the co-occurrence of other cloud types such as cirrus and rain clouds is minimal.

### 2.1. The CIRA Cloud and No Cloud Image Archive

> Producing a cloud composite climatology is conceptually simple but operationally time consuming [*Reinke et al*., 1992].

The set of hourly cloud maps derived from NOAA GOES data for meteorological purposes using the image processing method as described in *Combs et al*. [2004, 2010] was used for this study. The image processing method is repeated in condensed form below to support the informed use of FLCC indices. Users are encouraged to review the published methods for greater detail about the algorithms and the method in general. The image processing steps use data from three GOES channels to classify each pixel as clear sky, low cloud, or high cloud. As described in section 1.3 both temporal and spatial comparisons are needed to accurately differentiate clouds from the Earth and ocean surface. Crucial to the description below is the concept of a "month-hour." Due to Sun angle, thermal loading, and other conditions that change hourly throughout the day, satellite images taken at 10 A.M. local time during June will be more similar to each other than to images from June midafternoon. The June 10 A.M. images will also be more similar to July 9 A.M. images than to June midafternoon images. To improve the image classification process, image files are separated by month and by hour into month-hour groups.

The Cooperative Institute for Research in the Atmosphere (CIRA) ground station collects GOES data daily. The data are the same as those collected by other ground stations and available for download from NOAA CLASS. Data from June 1999 to September 2009 were used to derive hourly cloud maps for the study period.

Cloud classifications were generated using GOES West Imager sensor data from channel 1, visible wavelengths (0.55–0.75 μm); channel 2, shortwave infrared (3.6 μm); and channel 4, longwave infrared (10.7 μm) wavelengths. Channel 1 spatial resolution is 1 km, whereas channels 2 and 4 are 4 km. The 1 km channel 1 data were resampled to match the 4 km resolution of channels 2 and 4 after processing. Channel 1 data were compiled for daylight hours and channels 2 and 4 for all hours. Daytime imagery was classified using all three bands, whereas nighttime imagery, with no data in the visible channel, was classified using just the two infrared channels, shortwave channel 2 and longwave channel 4.

Low clouds tend to be the same temperature as the ground; however, their emissivity differs from the ground, especially at night. The difference in cloud emissivity is picked up by using two infrared bands each sensitive to energy transmitted within different wavelengths (3.6 μm or 10.7 μm). Solar energy, with its daily, seasonal, and interannual variation changes, changes the temperature of the Earth's surface. Matching image pairs by hour, month, and year, as described below, compares images with similar seasonal and time of day conditions. [*Jedlovec and Laws*, 2003].

Using the *Jedlovec and Laws* [2003] algorithm, channels 2 and 4 image files were matched according to time (an image pair for each hour of each month for each year) and divided into month-hour sets. For example, 30 channel 2 images were paired with their 30 temporally equivalent channel 4 images generating 30 image

**Table 2.** Temporal Summaries of GOES-Derived Hourly Fog and Low Cloud Data for the Dry Season (June–September) for 1999–2009

| Index Number | Index | Index Description[a] | Data Compression Ratio | Total Maps in Index |
|---|---|---|---|---|
| 1.1 | Summertime fog and low cloud cover frequency | Decadal (1999–2009[a]) average FLCC average hours/day for summer (June–September) | 26,352:1 | 1 |
| 1.2 | Total FLCC (1999–2009) | Total FLCC hours over summer over 9 years (1999–2009[a]) | 26,352:1 | 1 |
| 2.1 | Annual summer FLCC frequency | Average annual (1999–2009[a]) daily summer (June–September) | 2,928:1 | 9 |
| 2.2 | Total summer season FLCC (1999–2009) | Total FLCC hours each summer for 9 years (1999–2009[a]) | 2,928:1 | 9 |
| 3 | Diurnal summer season FLCC | Summer season FLCC h/12 h period (day and night) | 1,464:1 | 18[b,c] |
| 4 | Monthly FLCC | Total FLCC each month | 720 or 744:1 | 36[c] |
| 5 | Diurnal monthly FLCC | Monthly FLCC h/12 h period (day and night) | 360 or 372:1 | 36[b,c] |
| 6 | Hourly summer FLCC | For each summer, number of days with FLCC on an hourly basis | 122:1 | 216[c] |
| 7 | FLCC hourly by month | For each month, total number of day with FLCC on an hourly basis (e.g., 24 h/d) | 30 or 31:1 | 864[c] |

[a]There are two versions of all maps: "all clouds" (1999–2009) and "low clouds" (1999–2005); see text for further explanation.
[b]This is the number of maps per permutation (e.g., day or night).
[c]These maps are also available in "total hours" units.

pairs for the 1700 universal coordinate time (UTC) hour of June 2003 and 31 image pairs for 2300 UTC of July 2003. From each image pair, a difference value was calculated for each pixel by subtracting the 3.6 μm brightness temperature value from the 10.7 μm brightness temperature value. Next, three new image files are generated for each hour by selecting, from the 30 (or 31) image pairs, (1) the largest negative difference (LND), (2) the smallest positive difference (SPD), and (3) the warmest 10.7 μm temperature value (WTV) for each pixel location. These three image files were then used to perform two threshold tests. The first is the minimum difference test. If the 10.7 μm to 3.6 μm temperature difference value for a given pixel in an image pair is negative, and the difference is less than the LND value minus a threshold value (in this case 5.1 K over land, 4.1 K over ocean), it is tagged as cloud. Otherwise, it is considered clear. If the difference is positive and if the difference minus the SPD value is greater than the threshold value of 2.0 K, it is also tagged cloud. The second test is performed on all the "clear" pixels. If the 10.7 μm temperature for the pixel is 18.5 K colder than the WTV value, it is retagged cloud.

During daytime hours when visible channel 1 data are available, an additional test is used to catch any pixels that were misclassified as clear using the channel 2 and channel 4 difference test. Misclassification during the day can occur because shortwave channel 2 receives reflected shortwave solar radiation unlike nighttime conditions when only reemitted shortwave is received. This last test that uses the *Reinke et al*. [1992] method is performed on pixels classified clear in the previous steps. For each pixel location, all channel 1 images within a given month-hour set are compared and the minimum value (excluding values within suspected cloud shadow regions) is determined. This results in a cloud-free image called a "background." Then each image in the group is compared to the background image. Previous clear pixels were retagged cloudy if their value was greater than the background plus a threshold value for that location.

The final step was to assign cloud height. Each cloud pixel is further identified as "low" or "high" depending on whether the 10.7 μm temperature is below or above a threshold of 273 K. A pixel identified as high does not necessarily mean that there is not a low cloud below the high cloud, just that the satellite "sees" only the high cloud.

The GOES images were processed using the above algorithms written in Fortran to produce hourly cloud maps [*Combs et al*., 2004, 2010] and ingested into the geographic information system (GIS) conversion process as McIDAS area files.

### 2.2. Calculated Statistics

Each FLCC index (Table 2) is the result of a data compression of hourly classified image files into a single georeferenced digital raster. The value of each pixel in the raster (map) is the calculated result of spatial statistics routines coded as Python scripts and run in ArcMap (Environmental Systems Research Institute, ESRI, v10.2.2, 2014). Individual hourly image files from CIRA were used in their native binary format to quality control the indices and to identify specific image files to remove from the calculations. The most common reason for

**Table 3.** List of Locations With FLCC Spatial Patterns of Particular Interest

| Location Number | Location (North to South) |
|---|---|
| 1 | Eureka/Humboldt Bay |
| 2 | Cape Mendocino |
| 3 | Point Arena |
| 4 | Petaluma Gap |
| 5 | Point Reyes |
| 6 | Montara/Half Moon Bay |
| 7 | Año Nuevo |
| 8 | Monterey Bay |
| 9 | Salinas Valley |
| 10 | Big Sur Coast |
| 11 | Los Osos Peninsula |
| 12 | Point Arguello |

removal was poor image quality during dusk and dawn when extreme Sun angles impact brightness values. Substitutions for removed hour data were made by averaging the hour before and hour after.

Monthly averaged hour (month-hour) files from the CIRA archive for the summer season were converted into geographic information system (GIS) raster file format using McIDAS and the public domain *National Ocenographic and Atmospheric Administration* [2015] [*Ansari et al.*, 2010] and GIS software [*Environmental Systems Research Institute* (*ESRI*), 2014]. The summer season included September because it exhibits a combination of high temperatures and negligible rainfall, resulting in high cumulative water deficit. For years 2006–2009, image files with only a binary classification of cloud-no cloud (e.g., no low cloud class) were used in GIS processing.

Month-hour FLCC rasters for 1999–2005 (both high and low cloud classes) and 1999 through 2009 (one cloud class) were aggregated into seven different indices (Table 2) to investigate diurnal, monthly, seasonal, interannual, and decadal patterns. Diurnal indices are defined by two 12 h periods. Nighttime hours are 3:00 to

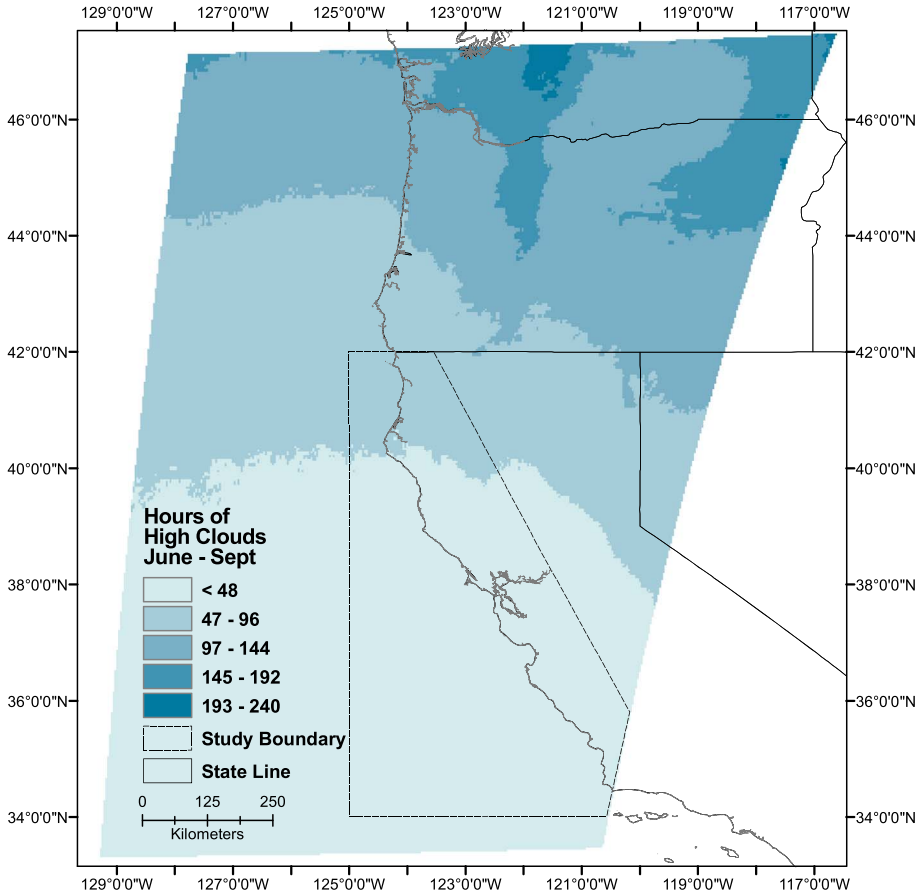


**Figure 1.** Hours of summer high clouds (June–September) averaged over six summers, 1999–2005. The majority of the California study area boundary (dashed line) has less than 48 h of summer high clouds (1%). The northern portion of the study area has up to 96 h of summer high clouds (3%).

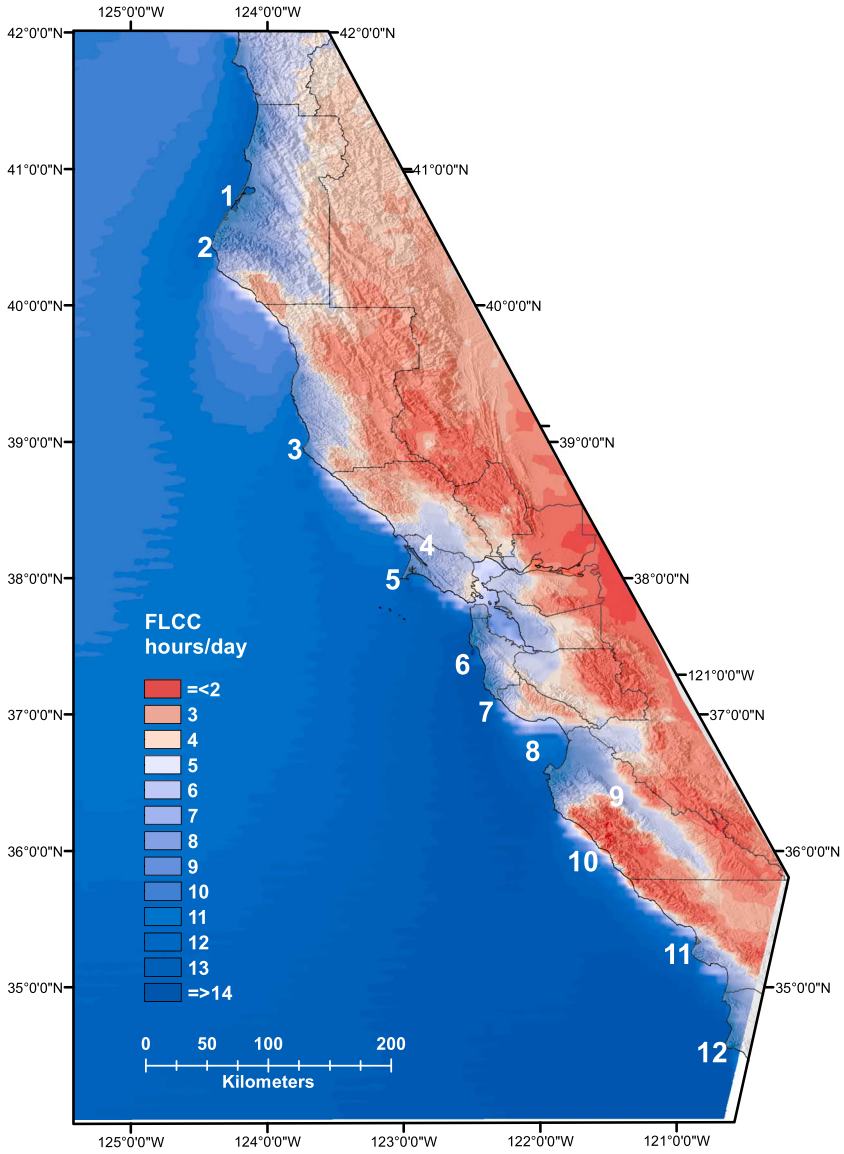


**Figure 2.** Decadal FLCC index. Mean FLCC h/d averaged over nine summer seasons (June–September, 1999–2000, 2002–2005, and 2007–2009) for the north and central California coast. Black outlines depict coastal counties, from north to south (and clockwise around the San Francisco Bay-Delta coastline): Del Norte, Humboldt, Mendocino, Sonoma, Marin, Napa, Solano, Contra Costa, Alameda, Santa Clara, San Mateo, San Francisco, Santa Cruz, Monterey, San Luis Obispo, and Santa Barbara. Numbered map locations are also listed in Table 3: 1 = Eureka/Humboldt Bay, 2 = Cape Mendocino, 3 = Point Arena, 4 = Petaluma Gap, 5 = Point Reyes, 6 = Montara/Half Moon Bay, 7 = Año Nuevo, 8 = Monterey Bay, 9 = Salinas Valley, 10 = Big Sur Coast, 11 = Los Osos Peninsula, and 12 = Point Arguello.

14:00 coordinated universal time (UTC), local time 7 P.M. to 6 A.M. Pacific daylight time (PDT). Daytime hours are 15:00 to 23:00 and 0:00 to 3:00 (7 A.M. to 6 P.M. PDT). Henceforth, local time will be used.

Data were missing for August 2001 and June 2006 leaving only nine full summers for interannual and decadal calculations. Monthly averages from all 11 years were used when available. Data compression ratios range from 26,352 h for the 9 year summertime FLCC index to 30 or 31 h for one month-hour index. Spatial patterns of interannual variability are characterized by standard deviation (SD) and coefficient of variation (CV).

Two groups of sites were selected to describe patterns found in the indices for the results and discussion sections. The first group, 12 generalized locations, was selected based on spatial and temporal patterns of interest (Table 3). The second group of six locations was selected for pixel-based time series analysis. Each

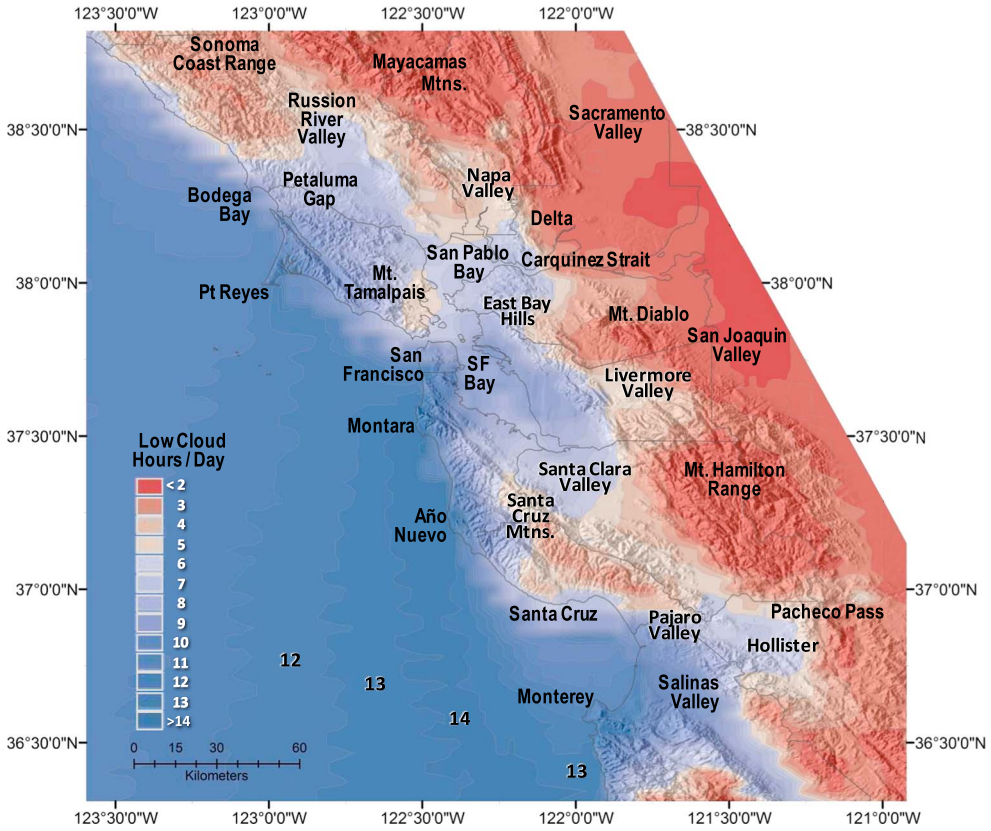


**Figure 3.** Close-up of decadal FLCC index for the San Francisco Bay Area; counties include, from north then along the San Francisco Bay-Delta coastline and continuing south, Sonoma, Marin, Napa, Solano, Contra Costa, Alameda, Santa Clara, San Mateo, San Francisco, Santa Cruz, and Monterey. Mean FLCC h/d averaged over nine summer seasons, (June–September, 1999–2000, 2002–2005, and 2007–2009). Contour lines for 12, 13, and 14 h/d are labeled in the southern oceanic portion of map.

pixel location corresponds to a colocation site where various fog-related research projects are being conducted [*Torregrosa et al.*, 2014].

### 2.3. Difference Map

To explore the impact on FLCC calculations using data that do not differentiate between high and low clouds, a difference map was generated using two data sets for the same six summers, 1999 to 2006. One data set quantified cloud cover based on three classes: clear sky and two cloud classes (high cloud and low cloud). The other data set quantified cloud cover using two classes: clear sky and cloud.

### 2.4. FLCC Contours and Elevation Profile

The 9 year summertime average FLCC raster (decadal index) was interpolated into a contour vector map using the ArcGIS Spatial Analyst functions with bilinear convolution [*ESRI*, 2014]. The contour map delineates 13 zones of FLCC from $<2$ hours per day (h/d) to more than 14 h/d. An exploratory analysis of the relationship between FLCC contours and elevation was conducted to expand and provide precision for the concept of a "fog belt." Elevation pixels with 270 m resolution were extracted along decadal FLCC h/d contour lines using the ArcGIS Zonal Histogram Spatial Statistics function [*ESRI*, 2014]. These were binned into 100 m elevation intervals to examine the elevation profile along an FLCC h/d contour.

## 3. Results

### 3.1. Low Versus High Cloud Cover

The difference map of low clouds subtracted from all clouds (Figure 1) shows a north-south gradient with more high clouds in the north and a curved west to southeast pattern. The latitudinal zonation corresponds

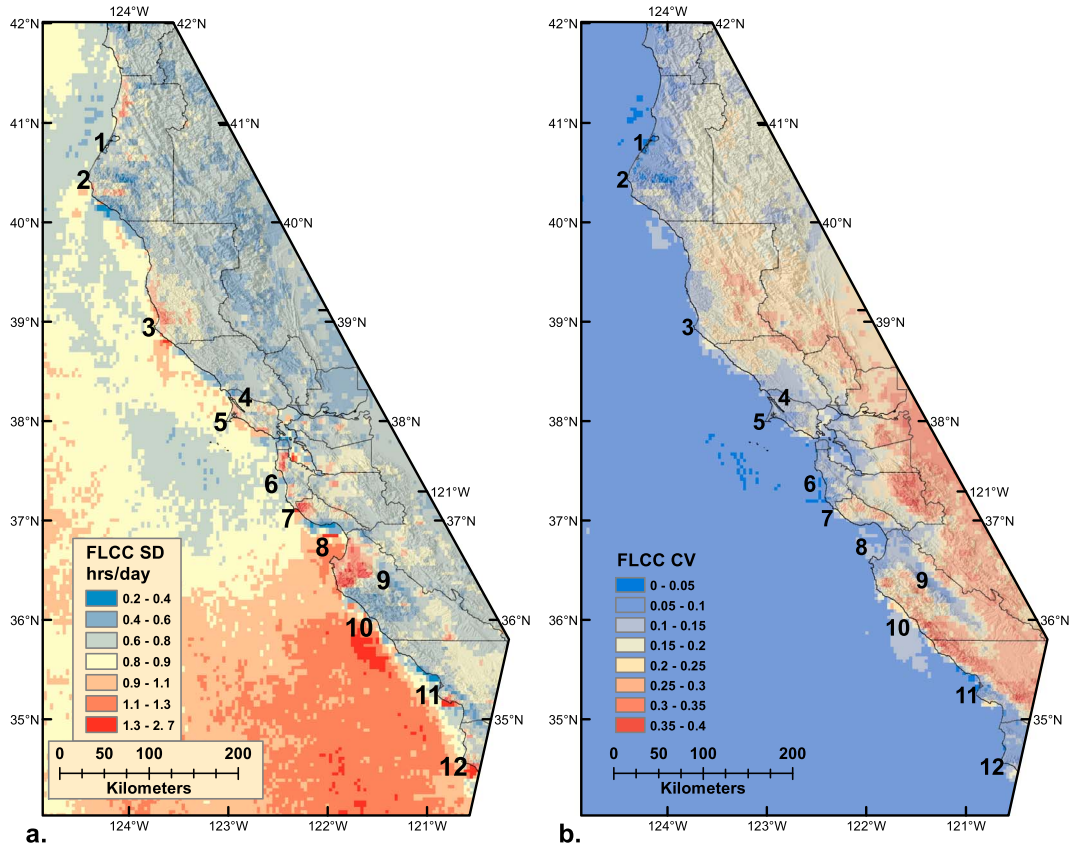


**Figure 4.** Interannual variation mapped across the landscape: (a) standard deviation and (b) coefficient of variation both derived from the decadal FLCC index of mean h/d for nine summers (June–September 1999–2001, 2002–2005, and 2007–2009). Geographic locations are numbered as in Figure 2 and Table 3.

to increased summer storms from the Pacific that contribute more high clouds at increasing latitude. The influence of the Cascades and Sierra Nevada mountain ranges, both situated at longitudes well inland from the study area, contributes to the curved pattern east of the study boundary. The majority of the California coast averages high clouds for less than 48 of the 2928 h of summer (1.6%). The north section of the coast averages 3% high cloud cover. As an average, high clouds contribute from 0.5 h/d in the south to 2.25 h/d at the Oregon border. Given the low occurrence of high clouds and the improved statistical robustness from using an additional 5 years of data, the 11 year single-cloud-class data set is used to explore FLCC patterns, except where specified. Subregions of particular interest, such as the San Francisco Bay Area, are in the zone least affected by high clouds during the summer.

### 3.2. Decadal Summertime FLCC Patterns

The decadal (1999–2009) summer FLCC index (Figure 2) for coastal north and central California shows a zone of FLCC incursion onto land. Twelve locations (Table 3) are used to describe localized patterns that form in response to specific interactions between the atmosphere, ocean, and land processes that drive FLC formation, movement, and dissipation. These locations will be referred to in the text by their location number (LN).

#### 3.2.1. Average FLCC Hours per Day

The decadal FLCC pattern over the ocean does not exhibit as much spatial variation as the FLCC pattern over land. In general, over the ocean and parallel to the coast, there is a NW to SE increase in FLCC h/d from 9 to 10 h/d at the 41° latitude to more than 14 h/d at the southern edge of the study area at the 34.5° latitude. The open ocean NW to SE pattern changes to a NE to SW pattern south of major capes such as Cape Mendocino (LN 2), Point Arena (LN 3), Point Reyes (LN 5), and Año Nuevo (LN 7). A similar NE to SW pattern also extends close to the Big Sur coast (LN 10) past Los Osos (LN 11). This latter NE to SW FLCC feature is parallel to a steep stretch of high-elevation coastal mountains abutting the ocean. The FLCC ocean contours near Humboldt Bay

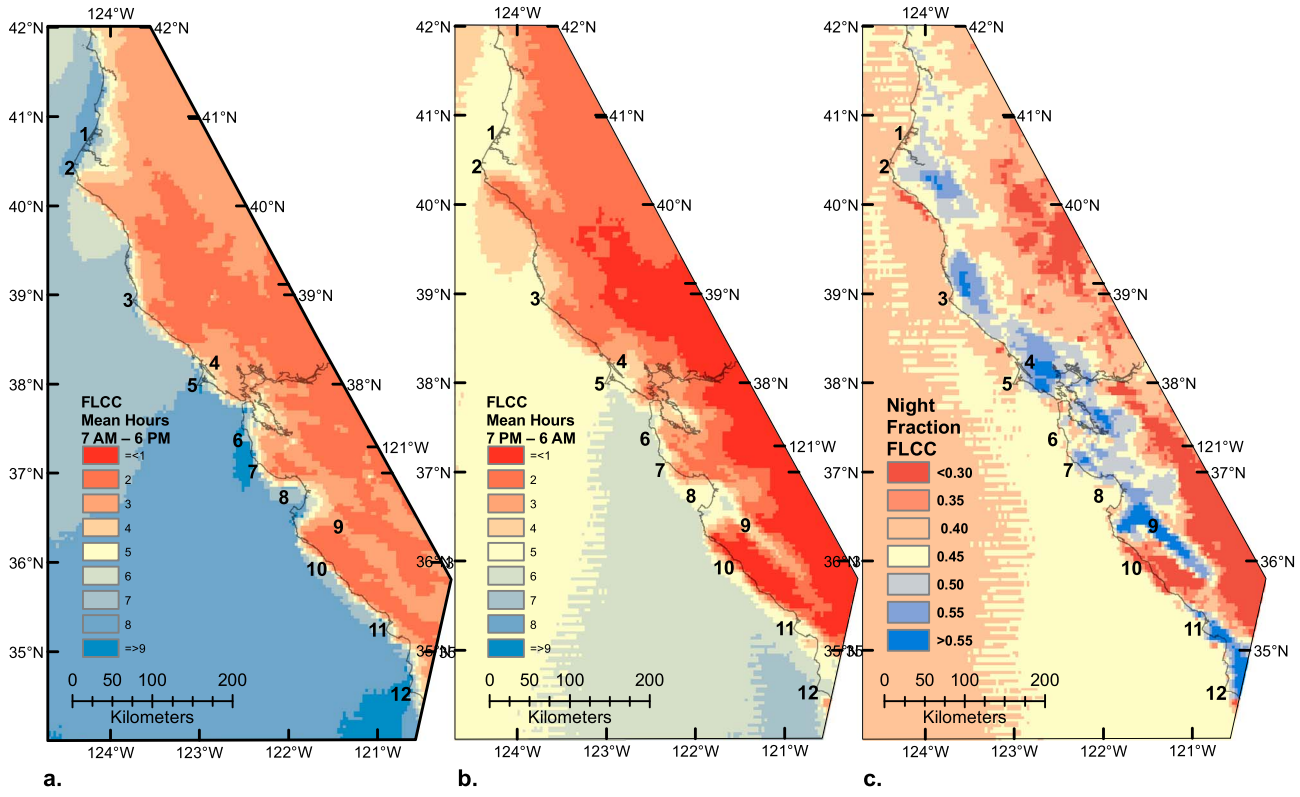


**Figure 5.** Diurnal pattern of decadal FLCC along the north and central California coast: (a) mean FLCC h/d for the 12 h/d period (7 A.M. to 6 P.M.), (b) the 12 h night period (7 P.M. to 6 A.M. local time), and (c) the fraction of FLCC that occurs at night. See Figure 1 for identification of counties outlined on the map and the seven numbered areas.

(LN 1) and along the San Mateo coast (LN 6 to LN 7) are similarly parallel; however, rather than increasing h/d bands NE to SW, FLCC increases from SW to NE, reaching >14 h/d at the coastline. The open ocean area with the least FLCC (8–9 h/d) is the large area south of Cape Mendocino (LN 2) extending well off the coast.

The FLCC patterns are more complex over land and out on the ocean within 20 km of land. FLCC patterns are strongly associated with terrain features and orientation of terrain to the prevailing NW wind. Stretches of coastline that face NW have the highest FLCC, Humboldt Bay (LN 1), Mendocino Coast north of Point Arena (LN 3), Point Reyes (LN 5), San Francisco-San Mateo Coast (LN 6 and LN 7), Monterey Peninsula/Salinas River mouth (LN 8 and LN 9), Morro Bay (near LN 11), and the Los Osos Peninsula north of Point Arguello (LN 12). Conversely, stretches of coastline with least FLCC are those facing SW, south, and in the lee of major capes, notably south of Cape Mendocino (LN 2), Point Arena (LN 3) to Bodega Bay (north of LN 5), Año Nuevo (LN 7) to Monterey (LN 10), and the Big Sur coast (LN 10) south of Monterey Bay.

The greatest inland incursion of FLCC is through low-elevation NW to SE valley systems open to the ocean. These long incursions include Humboldt Bay-Eel River (100 km, LN 1), Petaluma Gap-Russian River (75 km, LN 4), San Francisco Bay and offshoot valleys (maximum 85 km, between LN 5 and LN 6), Monterey Bay-Pajaro River (60 km, LN 8), Salinas River Valley (140 km, LN 9), and Los Osos-Santa Maria River (20+ km, LN 11 and beyond map extent).

Stretches of NW to SE oriented coastlines with high, steep mountains have very low FLCC. Three examples in the study area are the Big Sur coast (LN 10), the Sonoma coast north between Petaluma Gap (LN 4) and Point Arena (LN 3), and the southern end of the King Range south of Cape Mendocino (LN 2). Contrary to common perception, not all steep coastal mountains are good at blocking advecting marine stratus. The orientation and length of the mountainous stretch of coastline is important. Three areas with high steep coastal mountains that rise precipitously from the ocean have high FLCC including the northern 30 km stretch of the King Range next to Cape Mendocino (LN 2), the coastal mountains north (LN 5) of the entrance to San Francisco Bay (SF Bay), and south (LN 6) of the SF Bay entrance.

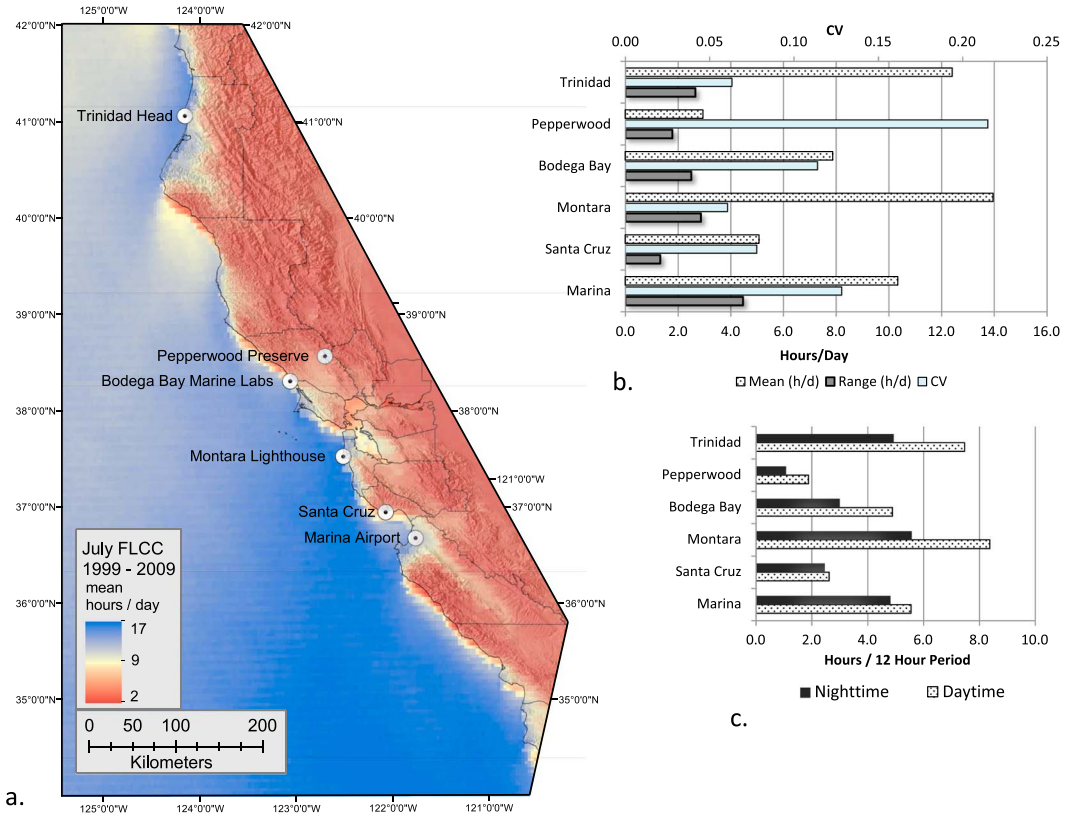


**Figure 6.** Site-based FLCC statistics at six locations. (a) Decadal average FLCC for the month of July (1999–2009) with six sites mapped from north to south: Trinidad Head, Pepperwood Preserve, Bodega Bay Marine Labs, Montara Lighthouse, Santa Cruz, and Marina Airport. (b) Interannual FLCC coefficient of variation, top scale, and bottom scale, hours per day, for decadal seasonal mean FLCC and decadal FLCC range (June–September) for nine summers (1999–2000, 2002–2005, and 2007–2009) for the six sites shown on map in Figure 6a. (c) Mean decadal FLCC for nighttime (7 P.M. to 6 A.M.) and daytime (7 A.M. to 6 P.M.) at six locations.

### 3.2.2. FLCC in Complex Terrain

A closer view of FLCC at the regional scale (Figure 3) shows a more complex pattern. The highest FLCC contour (>14 h/d) along the central coast touches land at Montara and Año Nuevo south of San Francisco. A series of mountainous barriers (listed clockwise) restricts the inland incursion of FLCC: Sonoma Coast Range, Mayacamas Mountains (Mtns), Mount Diablo, Mount Hamilton Range, Santa Cruz Mtns, and in the middle Mount Tamalpais. Between these barriers FLCC has highs of 13 h/d at three low-lying gaps closest to the ocean: Petaluma, San Francisco, and the coastal plains at the entrance to Salinas and Pajaro Valleys. Except for the low FLCC values in the shadow of Mount Tamalpais, FLCC is highest closest to the ocean and in a continuous line east and into valleys across from the gaps. Russian River and Santa Clara Valleys mirror each other with highs of 7 to 10 h/d. The East Bay Hills have high FLCC (9–10 h/d) due to their position east of the San Francisco gap along a straight line to the low-lying delta. Napa and Livermore Valleys, more distant from the ocean, have 5 h/d FLCC.

The Santa Cruz Mtns produce a complex fog pattern. The northern section of coast from Montara to Año Nuevo receives 9 to14 h/d, whereas the southern section of coast from Año Nuevo to Santa Cruz receives half that amount, 4 to 7 h/d. The northern section is west facing, whereas the southern section is SW to south facing. The higher elevations (400 to 1000+ m) of the southern Santa Cruz Mtns form a relatively fog free island (3 to 5 h/d) compared with the northern Santa Cruz Mtns (5 to 8 h/d). The bayside flatlands and foothills (<100 m) experience 9 h/d in the north and 4 h/d south toward the Santa Clara Valley.

The Santa Clara Valley also funnels fog south from San Francisco Bay with a gradient from 6 h/d at the south end of SF Bay to 3 h/d in Coyote Valley. The lower elevations (100 to 300 m) of the Mount Hamilton Range are still in the fog belt, but the higher elevations (>400 m) experience <3 h/d, similar to other highlands of the Inner Coast Range.

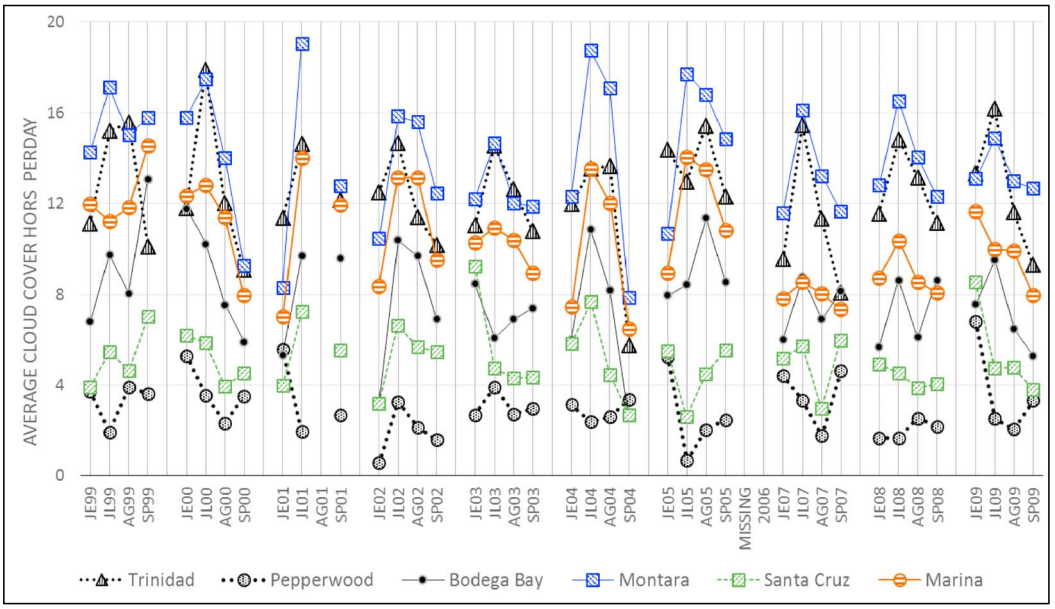


a.

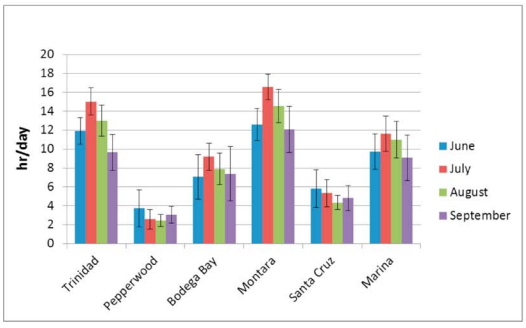


b.

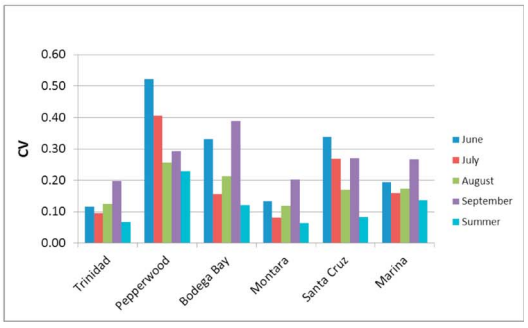


c.

**Figure 7.** Monthly variation (June–September) in FLCC at six sites over nine years, 1999–2000, 2002–2005, and 2007–2009. (a) Monthly mean FLCC h/d, (b) 9 year monthly mean FLCC, and (c) 9 year mean FLCC interannual CV.

### 3.2.3. Interannual Variability

The area of FLCC standard deviation (SD) that is highest (>2.5 h/d) and largest (Figure 4a) occurs over the ocean near the steep Big Sur coast (LN 10). The largest cluster of high SD on land occurs at the mouth of the Salinas Valley (LN 9) and continues offshore over Monterey Bay (LN 8). Smaller clusters of very high SD occur on the inland curving portion of SW facing coastal features (south of LN 3, LN 5, LN 7, LN 11, and LN 12). A few areas of moderately high SD (>0.9) are north of Point Arena (LN 3) and Humboldt Bay (LN 1). Coastal areas with the lowest SD are the same areas where average decadal FLCC is lowest (south of LN 2, Santa Cruz north of LN 8, and inland of LN 10) and the higher elevations east of LN 10 (Figure 2); however, not all areas of low FLCC have low SD.

The coefficient of variation (CV) provides a complementary measure of interannual variability as a function of FLCC (Figure 4b). Uniformly low CV (<0.10) occurs, in general, in areas with greatest FLCC (6 to 14 h/d, Figure 2). Along the immediate coast, the highest values of CV (>0.35) occur along the Big Sur coast (LN 10) almost to Los Osos (LN 11) where FLCC is low (<3 h/d). Moderately high CV (0.20 to 0.35) occurs where FLCC is low (3 to 4 h/d), and SD ranges from 0.75 to 1.0 h/d, except for the patch just south of Cape Mendocino (LN 2). Interannual CV is highest in the areas of lowest FLCC (<2 h/d), and SD < 0.5 h/d.

### 3.2.4. Diurnal Patterns

The FLCC daytime and nighttime pattern (Figure 5a) is different over ocean and land. Over the ocean FLCC is higher (6 to 9 h/d) during the day period than the night period (4 to 6 h/d), whereas over land, the range in

FLCC is equivalent during the two periods (5–9 h/d), but there is more land area that is covered with FLC (LN 4, LN 7, LN 9, LN 11, and LN 12). The nighttime fraction of FLCC shows this most clearly. When there is FLCC over land, it is present more often at night than during the day (Figure 5c). Nighttime fraction of FLCC is high (0.6) along most coastal areas with notable exceptions, the Big Sur coast (LN 10) and south of Cape Mendocino (LN 2).

### 3.3. Time Series at Selected Points

The time series analysis of FLCC month-hour means for June 1999 to September 2009 at six point locations (Figure 6a) shows strong spatial trends. Trinidad Head (Trinidad) represents the Humboldt Bay system. Bodega Bay Marine Labs (Bodega Bay) and Pepperwood Preserve (Pepperwood) span a regional coast-to-inland gradient. Montara Lighthouse (Montara), as previously described, is the landfall location for the highest contour of the decadal FLCC index. The Santa Cruz and Marina Airport (Marina) sites contrast conditions within Monterey Bay.

The statistical summary (Figure 6b) of seasonal averages shows that Pepperwood had the most interannual CV (0.215) and Trinidad the least (0.06); Marina had the greatest range (4.25 h/d) and Santa Cruz the least (1.3 h/d); and Montara had most FLCC (13.9 h/d) and Pepperwood the least (3 h/d). In contrast with the pattern of higher night fraction FLCC in inland areas with low mean FLCC (Figure 5c), all sites had more FLCC hours during the daytime period.

The monthly 9 year climatology for these sites (Figure 7a) provides more detail. Month-year FLCC h/d averages have a wider range than FLCC seasonal averages (Figure 6b). The site with the highest month-year FLCC was Montara in July 2001 (19 h/d), and the site with the lowest was Pepperwood in lowest relative monthly variability June 2002 (0.6 h/d). In general, Montara, Trinidad, and Marina have the highest FLCC h/d (Figure 7b). Pepperwood and Santa Cruz have the lowest FLCC h/d. Trinidad and Montara have the lowest relative monthly variability (Figure 7c). June and September are generally more variable across sites than July and August. The pattern of relative monthly variability is strongly site specific.

## 4. Discussion

The data presented here provide first-order FLCC climatology across the north and central California coast with high spatial resolution (~4 km), based on hourly satellite images. The spatial and temporal continuity of the data set is unique. Satellite observations provide wall-to-wall coverage of FLC, which eliminates the need for interpolation. Wall-to-wall coverage also provides a base for deriving statistical relationships with topography, synoptic meteorology, and other spatially explicit modeling methods and allows for the extraction of fog climatology and monthly time series at any point location within the landscape. The hourly time step and the ability to calculate total FLCC h/d contrast with other satellite records that take snapshots (i.e., daily MODIS at 10:30 and 14:30 [*Fischer et al*., 2009; *Sawaske and Freyberg*, 2014]) and do not resolve clouds at night when the majority of the deepest FLCC inland incursion occurs (Figure 5c). At the inland edge of FLCC incursion, FLCC often dissipates earlier than 10:30 A.M. and is therefore not fully captured by MODIS or AVHRR.

Point records, including airport observations and station data, have high temporal resolution but not continuous spatial coverage. Maps of FLCC zones based on high-frequency interpolated solar radiation data, such as the fog belt zones derived from the California Irrigation Management Information System (CIMIS) meteorological stations, tend to have coarse-scale spatial resolution (http://wwwcimis.water.ca.gov/Content/PDF/CimisRefEvapZones.pdf). Importantly, solar radiation measurements only resolve daytime clouds. Other sources, as discussed below, may provide ancillary information for better calibration and analysis of FLCC effects on temperature, humidity, and vegetation.

### 4.1. FLCC Spatial and Temporal Structure

#### 4.1.1. Terrain and Wind-Driven Patterns

Continuous FLCC coverage reveals many consistent spatial patterns. FLCC has generally been linked to topographic effects. We show in this study that indeed the primary factor for FLCC spatial pattern is topography; however, terrain feature placement with respect to wind direction and length of terrain feature is also of primary importance. Under the current decadal wind regime, terrain features less than 30 km do not tend to divert FLCC.

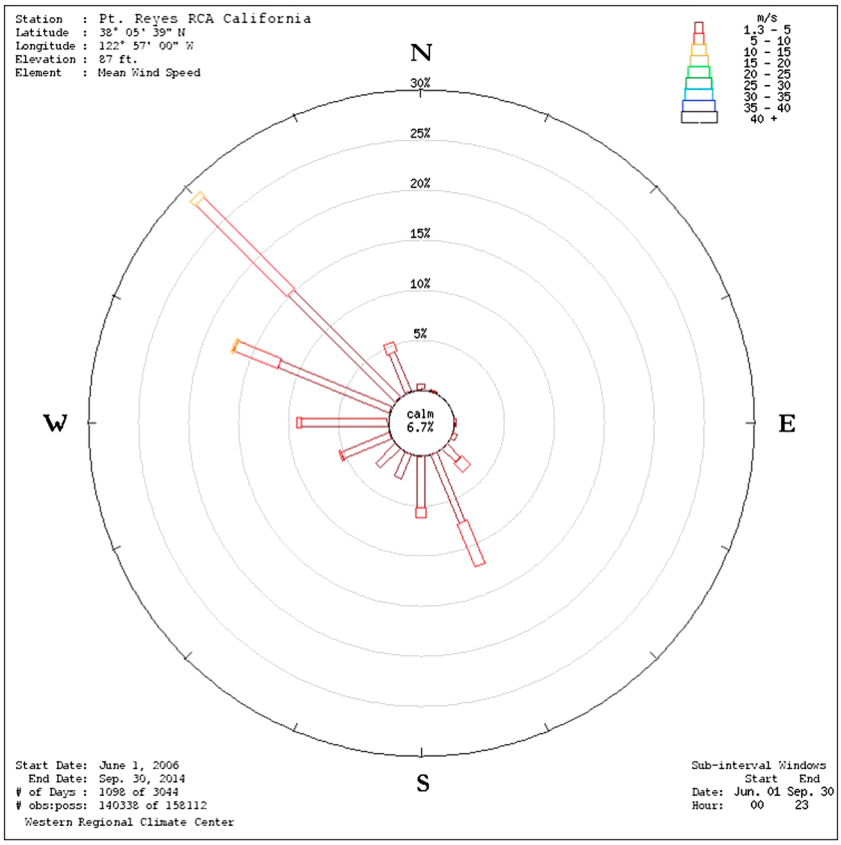


**Figure 8.** Wind Rose, Point Reyes, California. The predominant summertime wind direction is NW during the period of the GOES-derived cloud cover archive for 2000–2014.

Windward (W-NW facing) coastlines have more FLCC than leeward coastlines (SW-S). There are "FLCC shadows" downwind of major headlands/peninsulas, and these areas tend to have higher interannual variability (CV). The occurrence of FLCC in these pockets is reliant on southerly surges of FLCC, which irregularly occur through the summer in contrast with the strong prevailing W-NW winds. During June–September 2006 to 2014 at Point Reyes, the most exposed land station, W-NNW winds occur 60% of the time, but southerly (SSW-SE) winds occur 32% of the time (Figure 8) [*Western Regional Climate Center*, 2015]. Several authors have identified these southern surges with cyclonic vorticity resulting from a bend in the relative angle of the coastline producing changes in low-level wind speed and direction such as the Catalina eddy in the California Bight off the coast in Southern California and the recently named Santa Cruz eddy [*Archer et al.*, 2005; *Hu and Liu*, 2002; *Parish et al.*, 2013].

#### 4.1.2. FLCC Zones

The histogram of elevation pixels extracted along the 3 h/d FLCC contour of the Inner Coast Range south from 39.6 N (Figure 9a) shows a distinct dropoff in FLCC above 500 m, although the tail of the distribution extends above 1000 m. A similarly constructed histogram for the Santa Lucia Range (Figure 9b) shows a more gradual decline in the elevations along the 3 h/d FLCC contour, with the sharpest drop at $>$600 m, a tail extending to 1400 m, and highest elevations on the NW flank of the mountains downwind of the high fog Monterey Peninsula. These results are broadly consistent with the mechanisms [*Wood and Bretherton*, 2006; *Wood*, 2012] described above and the inversion heights reported by *Iacobellis and Cayan* [2013].

A comparison of annual average h/d FLCC derived from GOES with records of cloud ceilings below 400 m compiled by *Johnstone and Dawson* [2010] from Arcata and Monterey airport observations shows a strong and highly significant correlation between GOES-derived FLC and Monterey airport records with an intercept of $-1.66$ h and $p$ value of 0.0005 (Figure 10). The correlation with Arcata airport records is weak as expected given the higher amount of high clouds at that latitude (Figure 1). Our maps are also consistent with the spatially explicit results from *Iacobellis and Cayan* [2013].

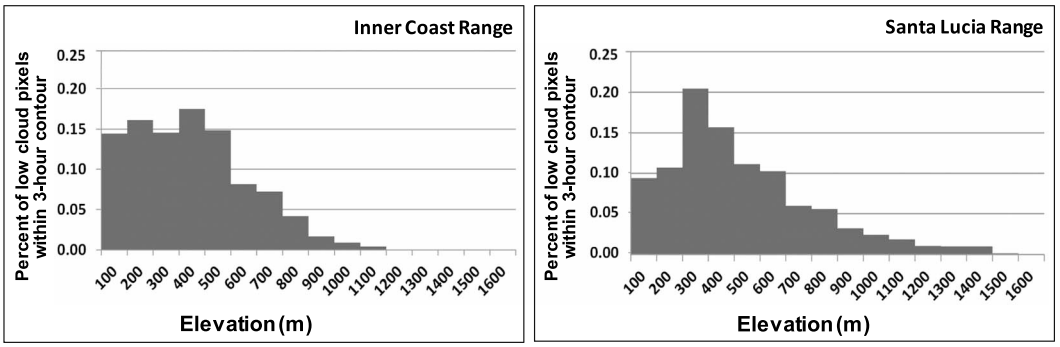


a. b.

**Figure 9.** Number of pixels extracted along the 3 h FLCC contour and binned into 100 m elevation bands (100 m to 1600 m) for (a) inner coast range and (b) Santa Lucia range.

The mechanisms described by *Wood and Bretherton* [2006] and *Wood* [2012] are consistent with the GOES-derived FLCC maps. Marine stratocumulus increases in frequency and lasts longer under the vertical barrier of a strong inversion that also acts to lower the FLC base heights. Inversion heights reported by *Johnstone and Dawson* [2010] averaged ~400 m, based on soundings at Oakland. Taken together, this information suggests that the landscape coherence in high interannual variability, expressed by the CV, (Figure 4b) at the inland limits is likely a function of inversion heights, whereas the high interannual variability expressed by the SD (Figure 4a) is more strongly related to the constraining topographic barrier to advection. Inversion heights vary through the season with the intensity of subsidence, often driven by upper level low-pressure systems that pass on an irregular basis. These systems first thicken the FLC layer, allowing higher-elevation incursions, but when inversion heights rise too high, FLC dissipate. Incursion into the higher elevations is limited to those periods when the inversion has lifted enough, but not too much. At the inland fringe, especially at lower elevations, a higher evaporative demand relative to cloud droplet condensation results in very low FLCC h/d beyond the San Francisco Bay-Delta across the Carquinez Strait. Each of the FLCC contour lines (Figures 2 and 3) represents the results of these interacting processes of FLC formation and dissipation and can be thought of as FLCC zones or more colloquially fog belt zones.

Visually integrating the geography of FLCC h/d contours of inland incursion in Figures 2 and 3 with the geography of CV reveals that the 3 h/d FLCC contour has the greatest correspondence with several delineations of fog belt zones documented by *Logan* [2006] and the fog belt zones in the CIMIS evapotranspiration map (http://wwwcimis.water.ca.gov/Content/PDF/CimisRefEvapZones.pdf).

Throughout this study the term FLCC has been used to aggregate advecting marine stratus, stratocumulus, and fog clouds that are visible from a satellite point of view. The FLCC data set presented in this study does not resolve the vertical structure of the clouds nor their distance from the ground. This data set does empirically resolve the inland limits and h/d zones of FLCC incursion. The results of GOES-derived FLCC are in line with results from other sources that do estimate vertical structure.

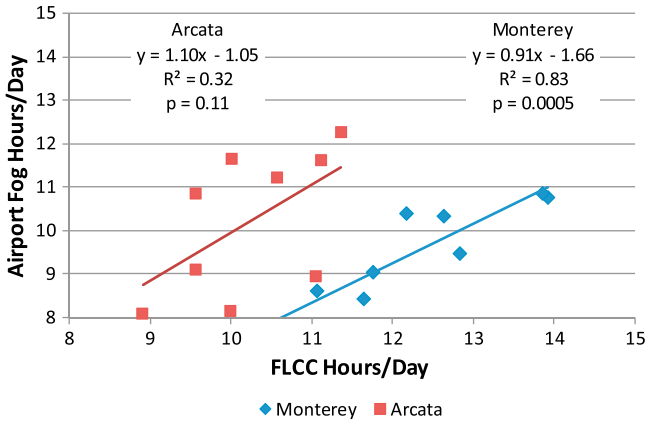


**Figure 10.** Correlation between airport observations of fog hours and satellite-derived FLCC per day at Arcata and Monterey.

### 4.1.3. Nighttime FLCC

Each FLCC index frames a specific period of time to reveal FLCC patterns that can be used to explore ecological mechanisms of interest (Table 1). The nighttime versus daytime pattern, although well known to meteorologists and anecdotally

to coastal residents, has not to our knowledge been previously quantified on a spatiotemporally continuous basis.

The strong pulse of nighttime FLCC into coastal ecosystems (Figure 5) provides an additional metric for delineating FLCC zones and suggests areas of expected fog cover. The pattern of high FLCC nighttime fraction, although similar to the spatial pattern of mean decadal FLCC h/d, has intriguing differences. Of the five areas with the highest FLCC h/d (Figure 2), Trinidad (LN 1), Montara (LN 6), Petaluma Gap (LN 4), Salinas Valley (LN 9), and Los Osos (LN 11), only Petaluma (LN 4) and Salinas (LN 9) have significantly high night fraction of FLCC. The opening to the San Francisco Bay through the Golden Gate has an unexpectedly low night fraction of FLCC. Nighttime FLCC incursion will bring a different set of impacts to ecosystem processes than daytime FLCC. The novel data set generated through this study will provide an opportunity to explore differences and help investigate the diurnal components of energy and water balance in these ecosystems. The vertical dimension of nighttime FLCC has received significant attention in Southern California with evidence suggesting that the observed reduction in fog frequency close to urban areas is associated with greater nighttime warming that raises ground level dew point temperature with subsequent lifting of cloud base heights [*Williams et al*., 2015].

### 4.2. Application of FLCC Indices

A primary motivator for developing FLCC indices was the need voiced by natural resource managers, fog water harvesters, farmers and vintners, and scientists for data that could be used to map FLCC across the landscape. The reported 33% reduction in fog over the last century [*Johnstone and Dawson*, 2010], although now placed in the context of known coupled cycles of ocean and atmosphere systems [*Johnstone and Mantua*, 2014], was startling and brought attention to the importance of retrieving FLCC records. The current California drought and increasing summer temperatures have heightened interest in understanding long-term and future trends of FLCC. The indices we have developed have many potential applications as well as limitations.

In a letter of support for the development of FLCC indices, Kirk Lenington, Senior Resource Planner, Mid-Peninsula Open Space District, sums up several potential uses for the indices.

"Spatial and temporal fog patterns significantly influence species distributions and ecological dynamics of California coastal ecosystems. The District owns over 8,000 acres of San Mateo County Coastland with a diverse range of plant and animal species, many of which are rare, threatened, or endangered. A historical reference of fog distribution and framework for long term fog monitoring system would greatly improve our ability to evaluate locations of unique or climatologically sensitive habitats, and develop more informed strategies for land management and future land acquisitions. Such products are particularly urgent given potential changes to fog patterns caused by climate change."

"Fog distribution information is also crucial for making well-informed decisions regarding native plant restorations. In cases where the District has acquired land with severe ecological disturbance, lack of information of fog frequency and location has made identifying target restoration species challenging. Products from (this) project would be of immediate use in determining the restoration objective for a disturbed site by selecting an appropriate nearby reference site that has similar fog patterns" (8 April 2011).

FLCC indices can be especially useful when merged with other data such as climatic water deficit (CWD) maps [*Flint and Flint*, 2014]. An overlap of FLCC and CWD maps would provide additional climatic resolution to identify areas of highest aridity, e.g., high CWD values and low FLCC values, from those of lesser aridity, e.g., high CWD and high FLCC. This information could be useful for habitat restoration. Other ancillary information such as data from ground fog monitoring stations would also improve the usefulness of FLCC indices to land managers.

FLCC indices are an aggregate of three types of clouds, those touching the ground (fog), fog as defined by airport observations (e.g., clouds with an aboveground base $<$400 m), and warm low clouds with an undetermined base height and a cloud top height usually below 1000 m (as previously described). The combination of a cloud touching the ground (fog) and high relative humidity does not always result in fog drip. Many factors influence the dynamics of water delivery from clouds: water droplet size and density, aerosol composition, wind speed, and all the atmospheric dynamics that affect an air parcel's trajectory and evolution [*Gonser et al*., 2012; *Wilkinson et al*., 2013; *Degefie et al*., 2015a, 2015b].

Under favorable conditions, fog drip can produce substantial local moisture for restoration and other uses [*Estrela et al*., 2009; *Domen et al*., 2014; *Katata*, 2014; *Batisha*, 2015]. Fog events vary in liquid water content and droplet size [*Yin et al*., 2014]. The amount of fog drip that will result from a fog event depends first on the relative exposure of the site where the fog cloud intercepts the land surface then on local topography and vegetation structure. Onshore winds drive a "conveyer-like belt" of clouds onto windward slopes, producing large amounts of fog drip. Leeward slopes have reduced fog drip [*Sawaske and Freyberg*, 2014].

Fog drip produced during the nighttime period can proceed with minimal evaporation. The elevation band between the cloud base and cloud top will be in contact with the land surface. Analysis of cloud base observations from airports and soundings colocated to the GOES data and a digital elevation model can identify areas of high potential fog drip. In addition to ameliorating summer drought for vegetation, fog drip hot spots can contribute enough moisture to affect low flows in coastal streams [*Sawaske and Freyberg*, 2014]. The identification of fog drip hot spots could inform vegetation management to maximize fog drip potential by retaining large trees that are particularly efficient at intercepting fog.

As mentioned earlier there are many potential uses for FLCC indices. One example that bears mention for its relevance to endangered species restoration activities, for the recently released Coho Salmon Recovery Plans for the Central California Coast and Northern California/Southern Oregon Coast [*National Marine Fisheries Service*, 2012], is the use of FLCC indices to identify areas where FLCC acts to strongly reduce incident solar radiation to streams and lower riparian evapotranspiration. The cascading effect of the shade and fog drip provided by FLCC includes increased low flows and reduced maximum stream temperatures in late summer. Steam temperature is a fundamental constraint on cold water fisheries, especially endangered coho salmon and threatened steelhead trout. FLCC indices could be used to identify areas with low long-term interannual variability and high FLCC h/d, two metrics that show promise as measures of climatic resilience.

### 4.3. Future Directions

Several future research areas that focus on improving FLCC indices have been identified in the preceding sections: integrating cloud ceiling height to improve the vertical dimension; extending the temporal period for the FLCC indices by adding earlier and more recent GOES data; and increasing the spatial resolution, perhaps through multisensor fusion. Other future research areas focus on the application of these indices or changing conditions that will affect the stationarity of FLCC indices such as global warming or the localized effects of urban heat island warming.

Millions of people live in coastal areas of California that are climatically influenced by FLCC. The term climatically influenced, for the purpose of this qualitative description, is defined as zones of decadal July FLCC index $>9$ h/d (Figure 6). In these areas, the difference in temperature between days with FLCC and days of no-cloud cover can be a matter of life or death. For more details about the higher proportion of fatalities that occurred among coastal residents during and after the July 2006 heat wave, see *Knowlton et al*. [2009].

Recently, record-breaking high temperatures were recorded on cloud-free 16 August 2015: 32°C in San Francisco and 40°C in Napa. On 21 August 2015, after several days of increasing FLCC, maximum temperatures had fallen back to 21°C in San Francisco and 22°C in Napa (http://www.timeanddate.com/weather/). Many are now asking: How will global climate change affect the frequency and distribution of FLCC? Although this climate change question could be thought of as just one of the many future directions for FLCC research, an approach that integrates many separate research directions may meet the challenge of answering this question more effectively.

An interdisciplinary approach for future research directions would have many of the same benefits as colocating disparate research projects. Spatially and temporally coincident measurements of individual system elements provide data not only for the individual system element but also for understanding system-level dynamics. Coincident measurement in a system dynamic context would advance our understanding of spatial and temporal patterns of FLCC on many fronts simultaneously.

FLCC patterns result from multiple interacting factors across multiple scales [*Koračin et al*., 2014; *Torregrosa et al*., 2014]. Recent work that quantified the connections between annual FLCC frequencies, sea surface temperature (SST), North Pacific high-pressure fields, inland temperature gradients, and other factors for the purpose of incorporating stratocumulus-forming processes into a regional climate model (RCM) at a 10 km scale shows promise [*O'Brien*, 2011; *O'Brien et al*., 2013]. *O'Brien's* [2011] was able to reproduce annual

historical patterns from *Johnstone and Dawson* [2010] and historical reanalysis as well as forecast fog frequency into the future. A downward trend emerged for all climate futures modeled. Similar global drivers and long-term historical trends have been observed from other coastal fog regions [*Garreaud*, 2011; *Haensler et al*., 2011; *Cermak*, 2012; *Schulz et al*., 2012; *Sugimoto et al*., 2013].

Forecasting future temporal and spatial variability and inland penetration patterns at resolutions comparable to those of this set of FLCC indices will require an analysis that links synoptic patterns, subsidence strength, and SST at finer temporal scales while capturing the variability in topography and vegetation at relevant spatial scales. Certain key synoptic indices, pressure fields and surface winds in particular, can be derived from GCM output and can provide, at minimum, projections of the directional trend in FLCC frequency. Correlating the GOES-derived FLCC record to the full spectrum of meteorological observations could provide details about the synoptic mechanisms behind the observed spatiotemporal variability on shorter time scales. Improved quantification of FLCC formation, evolution, and dissolution processes could then be used as input to global climate models as they evolve to incorporate diurnal and shorter period intervals.

Application of the FLCC is just beginning, while improvement of the FLCC indices will be ongoing. An application question that has arisen is whether the interannual stability of the spatial patterns found through the CV analysis could be used to identify climate refugia. If FLCC continues to form over the ocean and the onshore/offshore breeze continues to advect FLCC, then places that are currently the foggiest will likely continue to be the foggiest in the future. How much does the stability of FLCC heterogeneity contribute to California's status as a biodiversity hot spot? Geodiversity [*Anderson et al*., 2015] sets the stage for biodiversity, might areas that have stable and diverse FLCC values provide the bioclimatic variability to incubate species diversity?

Other questions that have arisen include the use of FLCC to pinpoint monitoring stations for indicators of climate change. This question has two conceptual branches. The first is the use of FLCC itself as an indicator. FLCC h/d contours at the "leading edge" of inland incursion might be good locations to monitor as these could be the most sensitive to climate change. Conversely, change in the areas with highest FLCC h/d may indicate larger synoptic influences. Atmospheric scientists would be needed to help weigh in on a monitoring design. The second conceptual branch is the use of FLCC patterns to identify locations for monitoring indicators of the factors that change the formation, evolution, and dissipation of FLCC. These would include additional monitoring buoys to increase the spatial resolution of ocean upwelling patterns, improved analysis and understanding of the onshore/offshore breezes across the SF Bay-Delta, additional wind/temperature profiler data in both horizontal and vertical dimensions along with improved mechanistic understanding of the interaction among layered air masses; and additional data on aerosol composition with improved understanding of sea spray, cloud condensation nuclei, and long-distance aerosol transport effect on FLCC. Dynamical downscaling of fog through RCMs is in its infancy; *O'Brien* [2011] was able to project a decrease in fog in 2061–2069 using the CCSM-A2 climate future, but it was necessary to statistically downscale SST using historical patterns to capture the California Current and upwelling that were not captured with the coarse-scale CCSM output.

## 5. Concluding Remarks

We were motivated to produce these data to satisfy the high demand from many different sectors for an easy to use data set that captures the influence of FLC and the complex topoclimatic patterns of the California coastal terrain [*Terjung et al*., 1969] for numerical analysis of coastal ecosystem processes. Unlike the current NOAA fog products that are based on absolute thresholds to differentiate low clouds from land and ocean, these data were derived using relative thresholds along both spatial and temporal dimensions, a more computationally demanding approach.

The digital data produced by this study will allow resource managers to ingest fog and low clouds into their spatial analyses and directly inform their management decisions. The nighttime component is a unique and strong point of this study. Daytime and nighttime maps of FLCC will help advance scientific research into FLCC impacts on managed and natural ecosystems. FLCC maps can be overlain directly into GIS to locate restoration areas for species that require the cool and moist conditions of persistent summertime low clouds. Viticulture managers can use the maps to identify new viticultural appellations such as the Petaluma Gap. Finally, researchers trying to understand the ecosystem service contribution of coastal fog will have indices to correlate FLC with stream temperatures at landscape levels, urban energy use, and human health effects.

**Acknowledgments**
FLCC indices can be downloaded from the California Landscape Conservation Cooperative Climate Commons, http://climate.calcommons.org/. We thank the California Landscape Conservation Cooperative, USGS Climate and Land Use Change Program, and the Gordon and Betty Moore Foundation for supporting the founding of the Pacific Coastal Fog Project and the 5 day workshop (Menlo Park, California, 2012) and Warren Blier, National Weather Service, San Francisco, for providing comments on earlier drafts of this manuscript. Any use of trade, firm, or product names is for descriptive purposes only and does not imply endorsement by the U.S. Government.

## References

American Meteorological Society (2014), Fog, Glossary of Meteorology. [Available at http://glossary.ametsoc.org/wiki/fog.]
Anderson, M. G., P. J. Comer, P. Beier, J. J. Lawler, C. A. Schloss, S. Buttrick, C. M. Albano, and D. P. Faith (2015), Case studies of conservation plans that incorporate geodiversity, *Conserv. Biol.*, *29*(3), 680–691, doi:10.1111/cobi.12503.
Ansari, S., S. Del Greco, and B. Hankins (2010), The weather and climate toolkit, Abstract IN32A-06 presented at 2014 Fall Meeting, AGU, San Francisco, Calif., 13–17 Dec.
Archer, C. L., M. Z. Jacobson, and F. L. Ludwig (2005), The Santa Cruz eddy. Part I: Observations and statistics, *Mon. Weather Rev.*, *133*(4), 767–782, doi:10.1175/mwr2885.1.
Azevedo, J., and D. L. Morgan (1974), Fog precipitation in coastal California forests, *Ecology*, 1135–1141, doi:10.2307/1940364.
Baguskas, S. A., S. H. Peterson, B. Bookhagen, and C. J. Still (2014), Evaluating spatial patterns of drought-induced tree mortality in a coastal California pine forest, *For. Ecol. Manage.*, *315*, 43–53, doi:10.1016/j.foreco.2013.12.020.
Bailey, R. G. (2009), Ecoregions of the United States, in *Ecosystem Geography*, pp. 93–114, Springer, New York, doi:10.1007/978-0-387-89516-1_7.
Barbour, M., J. Loidi, G. Garcia-Baquero, R. Meyer, S. Springs, and V. Whitworth (2014), The composition and physiognomy of forest types are strongly linked to distance inland along the northern California coast, *Phytocoenologia*, *44*(3–4), 165–173, doi:10.1127/0340-269x/2014/0044-0582.
Batisha, A. F. (2015), Feasibility and sustainability of fog harvesting, *Sustainability Water Qual. Ecol.*, doi:10.1016/j.swaqe.2015.01.002.
Beer, C. G., and L. B. Leopold (1947), Meteorological factors influencing air pollution in the Los Angeles area, *Eos Trans. AGU*, *28*(2), 173–192, doi:10.1029/TR028i002p00173.
Bendix, J., B. Thies, T. Nauß, and J. Cermak (2006), A feasibility study of daytime fog and low stratus detection with TERRA/AQUA-MODIS over land, *Meteorol. Appl.*, *13*(2), 111–125, doi:10.1017/s1350482706002180.
Borthagaray, A. I., M. A. Fuentes, and P. A. Marquet (2010), Vegetation pattern formation in a fog-dependent ecosystem, *J. Theor. Biol.*, *265*(1), 18–26, doi:10.1016/j.jtbi.2010.04.020.
California Department of Water Resources (2012), Reference Evapotranspiration Zones, Calif. Irrig. Manage. Inf. Syst., State of Calif., Nat. Resour. Agency. [Available at http://wwwcimis.water.ca.gov/Content/PDF/CimisRefEvapZones.pdf.]
Cannon, W. A. (1901), On the relation of redwoods and fog to the general precipitation in the redwood belt of California, *Torreya*, *1*(12), 137–139. [Available at http://www.jstor.org/stable/40594951.]
Carbone, M. S., A. P. Williams, A. R. Ambrose, C. M. Boot, E. S. Bradley, T. E. Dawson, S. M. Schaeffer, J. P. Schimel, and C. J. Still (2013), Cloud shading and fog drip influence the metabolism of a coastal pine ecosystem, *Global Change Biol.*, *19*, 484–497, doi:10.1111/gcb.12054.
Cereceda, P., M. Farías, P. Osses, R. S. Schemenauer, and H. Larrain (2003), Remote sensing methods and techniques to determine potential areas for fog water collection, paper presented at 11th International Rainwater Catchment Systems Association Conference, Texcoco, Mexico, Aug. [Available at http://www.eng.warwick.ac.uk/ircsa/pdf/11th/Cereceda.pdf.]
Cermak, J. (2012), Low clouds and fog along the South-Western African coast—Satellite-based retrieval and spatial patterns, *Atmos. Res.*, *116*, 15–21, doi:10.1016/j.atmosres.2011.02.012.
Chen, T., W. B. Rossow, and Y. Zhang (2000), Radiative effects of cloud-type variations, *J. Clim.*, *13*(1), 264–286, doi:10.1175/1520-0442(2000)013<0264:reoctv>2.0.co;2.
Collett, J. L., Jr., A. Bator, D. E. Sherman, K. F. Moore, K. J. Hoag, B. B. Demoz, X. Rao, and J. E. Reilly (2002), The chemical composition of fogs and intercepted clouds in the United States, *Atmos. Res.*, *64*, 29–40, doi:10.1016/s0169-8095(02)00077-7.
Combs, C. L., W. Blier, W. Strach, and M. DeMaria (2004), Exploring the timing of fog formation and dissipation over San Francisco Bay area using satellite cloud composites, Preprints, 13th Conf. on Satellite Meteorology and Oceanography, Norfolk, VA, Am. Meteorol. Soc., P4.12. [Available at http://ams.confex.com/ams/13SATMET/techprogram/paper_78778.htm.]
Combs, C. L., R. Mazur, J. Clark, M. Norquist, and D. Molenar (2010), An effort to improve marine stratus forecasts using satellite cloud climatologies for the Eureka, CA region, paper presented at 17th Conference on Satellite and Oceanography, Annapolis, Md, Sept. 30. [Available at https://usgs.illiad.oclc.org/illiad/GIM/illiad.dll?Action=10andForm=70Meteorology.]
Dawson, T. E. (1998), Fog in the California redwood forest: Ecosystem inputs and use by plants, *Oecologia*, *117*(4), 476–485, doi:10.1007/s004420050683.
Degefie, D. T., T. S. El-Madany, J. Hejkal, M. Held, J. C. Dupont, M. Haeffelin, and O. Klemm (2015a), Microphysics and energy and water fluxes of various fog types at SIRTA, France, *Atmos. Res.*, *151*, 162–175, doi:10.1016/j.atmosres.2014.03.016.
Degefie, D. T., T. S. El-Madany, M. Held, J. Hejkal, E. Hammer, J. C. Dupont, M. Haeffelin, E. Fleischer, and O. Klemm (2015b), Fog chemical composition and its feedback to fog water fluxes, water vapor fluxes, and microphysical evolution of two events near Paris, *Atmos. Res.*, *164–165*, 328–338, doi:10.1016/j.atmosres.2015.05.002.
Domen, J. K., W. T. Stringfellow, M. K. Camarillo, and S. Gulati (2014), Fog water as an alternative and sustainable water resource, *Clean Technol. Environ. Policy*, *16*(2), 235–249, doi:10.1007/s10098-013-0645-z.
Dorman, C. E., J. F. Mejia, and D. Koračin (2013), Impact of U.S. west coastline inhomogeneity and synoptic forcing on winds, wind stress, and wind stress curl during upwelling season, *J. Geophys. Res. Oceans*, *118*, 4036–4051, doi:10.1002/jgrc.20282.
Earles, J. M., O. Sperling, L. C. Silva, A. McElrone, C. Brodersen, M. North, and M. Zwieniecki (2015), Bark water uptake promotes localized hydraulic recovery in coastal redwood crown, *Plant Cell Environ.*, doi:10.1111/pce.12612.
Ellrod, G. P. (1995), Advances in the detection and analysis of fog at night using GOES multispectral infrared imagery, *Weather Forecasting*, *10*(3), 606–619, doi:10.1175/1520-0434(1995)010<0606:aitdaa>2.0.co;2.
Environmental Systems Research Institute (ESRI) (2014), ArcGIS Desktop: Release 10, Environ. Syst. Res. Inst., Redlands, Calif.
Estrela, M. J., J. A. Valiente, D. Corell, D. Fuentes, and A. Valdecantos (2009), Prospective use of collected fog water in the restoration of degraded burned areas under dry Mediterranean conditions, *Agric. For. Meteorol.*, *149*(11), 1896–1906, doi:10.1016/j.agrformet.2009.06.016.
Federal Aviation Administration (2013), *Federal Aviation Regulations/Aeronautical Information Manual*, Gov. Print. Off., Newcastle, Wash.
Filonczuk, M. K., D. R. Cayan, and L. G. Riddle (1995), Variability of marine fog along the California coast, SIO Reference No. 95-2, 102 pp.
Fischer, D. T., C. J. Still, and A. P. Williams (2009), Significance of summer fog and overcast for drought stress and ecological functioning of coastal California endemic plant species, *J. Biogeogr.*, *36*, 783–799, doi:10.1111/j.1365-2699.2008.02025.x.
Flint, L. E., and A. L. Flint (2014), California Basin Characterization Model: A dataset of historical and future hydrologic response to climate change, U.S. Geological Survey data release, doi:10.5066/F76T0JPB.
García-Reyes, M., and J. L. Largier (2012), Seasonality of coastal upwelling off central and northern California: New insights, including temporal and spatial variability, *J. Geophys. Res.*, *117*, C03028, doi:10.1029/2011JC007629.
Garreaud, R. D. (2011), The climate of northern Chile: Mean state, variability and trends, *Rev. Mex. Astron. Astrofis.*, *41*, 5.

Gershunov, A., and Z. Johnston (2011), The California heat wave 2006 with impacts on statewide medical emergency: A space-time analysis, *Geogr. Res. Forum*, *31*, 6–31.
Gilliam, H. (2002), *Weather of the San Francisco Bay Region, California Natural History Guides*, vol. 63, Univ. of Calif. Press, Oakland, Calif.
Gonser, S. G., O. Klemm, F. Griessbaum, S. C. Chang, H. S. Chu, and Y. J. Hsia (2012), The relation between humidity and liquid water content in fog: An experimental approach, *Pure Appl. Geophys.*, *169*(5–6), 821–833, doi:10.1007/s00024-011-0270-x.
Gundel, L. A., W. H. Benner, and A. D. A. Hansen (1994), Chemical composition of fog water and interstitial aerosol in Berkeley, California, *Atmos. Environ.*, *28*(16), 2715–2725, doi:10.1016/1352-2310(94)90443-x.
Gurnell, A. M. (1976), A note on the contribution of fog drip to streamflow, *Weather*, *31*, 121–126, doi:10.1002/j.1477-8696.1976.tb04414.x.
Haensler, A., J. Cermak, S. Hagemann, and D. Jacob (2011), Will the southern African west coast fog be affected by future climate change? Results of an initial fog projection using a regional climate model, *Erdkunde*, *65*, 261–275.
Harr, R. D. (1982), Fog drip in the Bull Run municipal watershed, Oregon, *Water Resour. Bull.*, *18*, 785–789, doi:10.1111/j.1752-1688.1982.tb00073.x.
Helmuth, B., B. R. Broitman, C. A. Blanchette, S. Gilman, P. Halpin, C. D. Harley, M. J. O'Donnell, B. Hofmann, and D. Strickland (2007), Mosaic patterns of thermal stress in the Rocky Intertidal Zone, *Bull. Ecol. Soc. Am.*, *88*(1), 40–45, doi:10.1890/0012-9615(2006)076[0461:mpotsi]2.0.co;2.
Herckes, P., K. T. Valsaraj, and J. L. Collett Jr. (2013), A review of observations of organic matter in fogs and clouds: Origin, processing and fate, *Atmos. Res.*, *132*, 434–449, doi:10.1016/j.atmosres.2013.06.005.
Hiatt, C., D. Fernandez, and C. Potter (2012), Measurements of fog water deposition on the California central coast, *Atmos. Clim. Sci.*, *2*, 525–531, doi:10.4236/acs.2012.24047.
Houze, R. A., Jr. (2014), *Cloud Dynamics International Geophysics*, vol. 104, pp. 1–432, Academic, Elsevier.
Hu, H., and W. T. Liu (2002), QuikSCAT reveals the surface circulation of the Catalina Eddy, *Geophys. Res. Lett.*, *29*(17), 1821, doi:10.1029/2001GL014203.
Iacobellis, S. F., and D. R. Cayan (2013), The variability of California summertime marine stratus: Impacts on surface air temperatures, *J. Geophys. Res. Atmos.*, *118*, 9105–9122, doi:10.1002/jgrd.50652.
Jedlovec, G. (2009), Automated detection of clouds in satellite imagery, in *Advances in Geoscience and Remote Sensing*, edited by G. Jedlovec, pp. 303–316, InTech, Rijeka, Croatia, doi:10.5772/46139.
Jedlovec, G. J., and K. Laws (2003), GOES cloud detection at the Global Hydrology and Climate Center, paper P1 presented at 12th conference on satellite meteorology and oceanography, Am. Meteorol. Soc., Long Beach, Canada, Feb.
Jedlovec, G. J., S. L. Haines, and F. J. LaFontaine (2008), Spatial and temporal varying thresholds for cloud detection in GOES imagery, *IEEE Trans. Geosci. Remote Sens.*, *46*(6), 1705–1717, doi:10.1109/TGRS.2008.916208.
Jensen, M. P., A. M. Vogelmann, W. D. Collins, G. J. Zhang, and E. P. Luke (2008), Investigation of regional and seasonal variations in marine boundary layer cloud properties from MODIS observations, *J. Clim.*, *21*(19), 4955–4973, doi:10.1175/2008jcli1974.1.
Johnstone, J. A., and T. E. Dawson (2010), Climatic context and ecological implications of summer fog decline in the coast redwood region, *Proc. Natl. Acad. Sci. U.S.A.*, *107*(10), 4533–4538, doi:10.1073/pnas.0915062107.
Johnstone, J. A., and N. J. Mantua (2014), Atmospheric controls on northeast Pacific temperature variability and change, 1900–2012, *Proc. Natl. Acad. Sci. U.S.A.*, *111*(40), 14,360–14,365, doi:10.1073/pnas.1318371111.
Kann, A., T. Schellander-Gorgas, and C. Wittmann (2015), Enhanced short-range forecasting of sub-inversion cloudiness in complex terrain, *Atmos. Sci. Lett.*, *16*(1), 1–9, doi:10.1002/asl2.511.
Katata, G. (2014), Fogwater deposition modeling for terrestrial ecosystems: A review of developments and measurements, *J. Geophys. Res. Atmos.*, *119*, 8137–8159, doi:10.1002/2014JD021669.
Katata, G., H. Nagai, M. Kajino, H. Ueda, and Y. Hozumi (2010), Numerical study of fog deposition on vegetation for atmosphere–land interactions in semi-arid and arid regions, *Agric. For. Meteorol.*, *150*(3), 340–353, doi:10.1016/j.agrformet.2009.11.016.
Knowlton, K., M. Rotkin-Ellman, G. King, H. G. Margolis, D. Smith, G. Solomon, R. Trent, and P. English (2009), The 2006 California heat wave: Impacts on hospitalizations and emergency department visits, *Environ. Health Perspect.*, *117*(1), 61–67, doi:10.1289/ehp.11594.
Koračin, D., J. A. Businger, C. E. Dorman, and J. M. Lewis (2005), Formation, evolution, and dissipation of coastal sea fog, *Boundary Layer Meteorol.*, *117*(3), 447–478, doi:10.1007/s10546-005-2772-5.
Koračin, D., C. E. Dorman, J. M. Lewis, J. G. Hudson, E. M. Wilcox, and A. Torregrosa (2014), Marine fog: A review, *Atmos. Res.*, *143*, 142–175, doi:10.1016/j.atmosres.2013.12.012.
LaDochy, S., and M. Witiw (2012), The continued reduction in dense fog in the southern California region: Possible causes, *Pure Appl. Geophys.*, *169*(5–6), 1157–1163, doi:10.1007/s00024-011-0366-3.
Lee, T. F., F. J. Turk, and K. Richardson (1997), Stratus and fog products using GOES-8-9 3.9-μm data, *Weather Forecast.*, *12*(3), 664–677, doi:10.1175/1520-0434(1997)012<0664:safpug>2.0.co;2.
Leipper, D. F. (1994), Fog on the U.S. west coast: A review, *Bull. Am. Meteorol. Soc.*, *75*(2), 229–240, doi:10.1175/1520-0477(1994)075<0229:fotuwc>2.0.co;2.
Lester, P. F. (1985), Studies of the marine inversion over the San Francisco Bay Area: A summary of the work of Albert Miller, 1961–1978, *Bull. Am. Meteorol. Soc.*, *66*(11), 1396–1402, doi:10.1175/1520-0477(1985)066<1396:sotmio>2.0.co;2.
Lilly, D. K. (1968), Models of cloud-topped mixed layers under a strong inversion, *Q. J. R. Meteorol. Soc.*, *94*(401), 292–309.
Limm, E. B., K. S. Simonin, A. G. Bothman, and T. E. Dawson (2009), Foliar water uptake: A common water acquisition strategy for plants of the redwood forest, *Oecologia*, *161*, 449–459, doi:10.1007/s00442-009-1400-3.
Logan, B. (2006), A statistical examination of the Climatic Human Expert System: The Sunset Garden Zones for California, Master's thesis, ETD etd-05082006-113632, Va. Polytech. Inst. and State Univ.
Madej, M. A. (2010), Analysis of trends in climate, streamflow, and stream temperature in north coastal California, paper presented at The Fourth Interagency Conference on Research in the Watersheds, Fairbanks, Alaska, 26–30 Sept.
Madej, M. A., C. Currens, V. Ozaki, J. Yee, and D. G. Anderson (2006), Assessing possible thermal rearing restrictions for juvenile coho salmon (oncorhynchus kisutch) through thermal infrared imaging and in-stream monitoring, Redwood Creek, California, *Can. J. Fish. Aquat. Sci.*, *63*, 1384–1396, doi:10.1139/F06-043.
Mass, C. F., M. D. Albright, and D. J. Brees (1986), The onshore surge of marine air into the Pacific Northwest: A coastal region of complex terrain, *Mon. Weather Rev.*, *114*, 2602–2627, doi:10.1175/1520-0493(1986)114<2602:tosoma>2.0.co;2.
Mislan, K. A. S., D. S. Wethey, and B. Helmuth (2009), When to worry about the weather: Role of tidal cycle in determining patterns of risk in intertidal ecosystems, *Global Change Biol.*, *15*(12), 3056–3065, doi:10.1111/j.1365-2486.2009.01936.x.
Mooney, H. A., M. T. K. Arroyo, W. J. Bond, J. Canadell, R. J. Hobbs, S. Lavorel, and R. P. Neilson (2001), Mediterranean-climate ecosystems, in *Global Biodiversity in a Changing Environment*, pp. 157–199, Springer, New York, doi:10.1007/978-1-4613-0157-8_9.
National Marine Fisheries Service (2012), Final recovery plan for central California coast coho salmon evolutionarily significant unit Natl. Mar. Fish. Serv., Southwest Reg., Santa Rosa, Calif.

National Oceanographic and Atmospheric Administration (2015), NOAA's Weather and Climate Toolkit. [Available at http://www.ncdc.noaa.gov/wct/.]
Nicholson, S. E. (2011), *Dryland Climatology*, Cambridge Univ. Press, New York, doi:10.1017/cbo9780511973840.
Norman, S. P., J. M. Varner, L. Arguello, and S. Underwood (2009), Fire and fuels management in coast redwood forests, Joint Fire Sci. Program Rep. 06-2-1-59. [Available at http://www.firescience.gov/projects/06-2-1-59/project/06-2-1-59_jfsp_final_report_06-2-1-59.pdf, accessed November 7, 2013.]
O'Brien, T. A. (2011), The recent past and possible future decline of California coastal fog, PhD thesis, Univ. of Calif., Santa Cruz. [Available at http://gradworks.umi.com/34/71/3471817.html.]
O'Brien, T. A., L. C. Sloan, P. Y. Chuang, I. C. Faloona, and J. A. Johnstone (2013), Multidecadal simulation of coastal fog with a regional climate model, *Clim. Dyn.*, *40*(11–12), 2801–2812, doi:10.1007/s00382-012-1486-x.
Palmer, A. K. (1917), Fog along the California coast, *Mon. Weather Rev.*, *45*, 496, doi:10.1175/1520-0493(1917)45<496:fatcc>2.0.co;2.
Parish, T. R., D. A. Rahn, and D. Leon (2013), Airborne observations of a Catalina eddy, *Mon. Weather Rev.*, *141*(10), 3300–3313, doi:10.1175/mwr-d-13-00029.1.
Pilié, R. J., E. J. Mack, C. W. Rogers, U. Katz, and W. C. Kocmond (1979), The formation of marine fog and the development of fog-stratus systems along the California coast, *J. Appl. Meteorol.*, *18*(10), 1275–1286, doi:10.1175/1520-0450(1979)018<1275:TFOMFA>2.0.CO;2.
Platnick, S., M. D. King, S. A. Ackerman, W. P. Menzel, B. A. Baum, J. C. Riédi, and R. A. Frey (2003), The MODIS cloud products: Algorithms and examples from Terra, *IEEE Trans. Geosci. Remote Sens.*, *41*(2), 459–473, doi:10.1109/tgrs.2002.808301.
Pruppacher, H. R., and J. D. Klett, (2010), Cooling of moist air, in *Microphysics of Clouds and Precipitation, Springer Atmospheric and Oceanographic Sciences Library*, vol. 18, pp. 485–501, Springer, New York, doi:10.1007/978-0-306-48100-0.
Redmond, K. T., and J. T. Abatzoglou (2014), Chapter 2. Current Climate and Recent Trends, in *Climate Change in North America, Regional Climate Studies*, edited by G. Ohring, Springer International Publishing, Switzerland, doi:10.1007/978-3-319-03768-4_2.
Reinke, D. L., C. L. Combs, S. Q. Kidder, and T. H. VonderHarr (1992), Satellite cloud composite climatologies: A new high-resolution tool in atmospheric research and forecasting, *Bull. Am. Meteorol. Soc.*, *73*, 278–285, doi:10.1175/1520-0477(1992)073<0278:scccan>2.0.co;2.
Santek, D. A., T. Whittaker, B. Hibbard, G. Dengel, D. Parker, and T. Rink (2006), McIDAS-V and OpenADDE: The next generation of McIDAS, paper presented at 22nd International Conference on Interactive Information Processing Systems for Meteorology, Oceanography, and Hydrology, Atlanta, Ga.
Sawaske, S. R., and D. L. Freyberg (2014), Fog, fog drip, and streamflow in the Santa Cruz Mountains in the California Coast Range, *Ecohydrology*, *8*, 695–713, doi:10.1002/eco.1537.
Schulz, N., J. P. Boisier, and P. Aceituno (2012), Climate change along the arid coast of northern Chile, *Int. J. Climatol.*, *32*(12), 1803–1814, doi:10.1002/joc.2395.
Schwartz, R. E., A. Gershunov, S. F. Iacobellis, and D. R. Cayan (2014), North American west coast summer low cloudiness: Broadscale variability associated with sea surface temperature, *Geophys. Res. Lett.*, *41*, 3307–3314, doi:10.1002/2014GL059825.
Seo, H., K. H. Brink, C. E. Dorman, D. Koracin, and C. A. Edwards (2012), What determines the spatial pattern in summer upwelling trends on the U.S. West Coast?, *J. Geophys. Res.*, *117*, C08012, doi:10.1029/2012JC008016.
Shreve, F. (1927), The vegetation of a coastal mountain range, *Ecology*, *8*, 27, doi:10.2307/1929384.
Slatyer, R. O. (1960), Absorption of water by plants, *Bot. Rev.*, *26*, 331–392, doi:10.1007/bf028608072.
Sugimoto, S., T. Sato, and K. Nakamura (2013), Effects of synoptic-scale control on long-term declining trends of summer fog frequency over the Pacific side of Hokkaido Island, *J. Appl. Meteorol. Climatol.*, *56*, 2242–2264, doi:10.1175/jamc-d-12-0192.1.
Taylor, S. V., D. R. Cayan, N. E. Graham, and K. P. Georgakakos (2008), Northerly surface winds over the eastern North Pacific Ocean in spring and summer, *J. Geophys. Res.*, *113*, D02110, doi:10.1029/2006JD008053.
Terjung, W. H., R. N. Kickert, R. J. Kochevar, J. P. Mrowka, S. O. Ojo, G. L. Potter, and S. E. Tuller (1969), The annual march of the topoclimatic spatial patterns of net radiation in southern California, *Arch. Meteorol., Geophys. Bioklimatol., Ser. B*, *17*(1), 21–50, doi:10.1007/bf02248858.
Torregrosa, A., M. D. Taylor, L. E. Flint, and A. L. Flint (2013), Present, future, and novel bioclimates of the San Francisco, California region, *PLoS One*, *8*(3), e58450, doi:10.1371/journal.pone.0058450.
Torregrosa, A., T. A. O'Brien, and I. C. Faloona (2014), Coastal fog, climate change, and the environment, *Eos Trans. AGU*, *95*(50), 473–474, doi:10.1002/2014EO500001.
Trenberth, K. E., and J. W. Hurrell (1994), Decadal atmosphere-ocean variations in the Pacific, *Clim. Dyn.*, *9*(6), 303–319, doi:10.1007/bf00204745.
Trenberth, K. E., J. T. Fasullo, and J. Kiehl (2009), Earth's global energy budget, *Bull. Am. Meteorol. Soc.*, *90*(3), 311–323, doi:10.1175/2008bams2634.1.
Valiente, J. A., M. J. Estrela, D. Corell, D. Fuentes, A. Valdecantos, and M. J. Baeza (2011), Fog water collection and reforestation at a mountain location in a western Mediterranean basin region: Air-mass origins and synoptic analysis, *Erdkunde*, *65*, 277–290, doi:10.3112/erdkunde.2011.03.05.
Vasey, M. C., V. T. Parker, K. D. Holl, M. E. Loik, and S. Hiatt (2014), Maritime climate influence on chaparral composition and diversity in the coast range of central California, *Ecol. Evol.*, *4*(18), 3662–3674, doi:10.1002/ece3.1211.
Weathers, K. C. (1999), The importance of cloud and fog in the maintenance of ecosystems, *Trends Ecol. Evol.*, *14*(6), 214–215, doi:10.1016/s0169-5347(99)01635-3.
Weathers, K. C., G. M. Lovett, G. E. Likens, and N. F. Caraco (2000), Cloudwater inputs of nitrogen to forest ecosystems in southern Chile: Forms, fluxes, and sources, *Ecosystems*, *3*(6), 590–595, doi:10.1007/s100210000051.
Western Regional Climate Center (2015), WRCC Wind Rose Summary Form. [Retrieved 1 Dec 2015 from http://www.wrcc.dri.edu/cgi-bin/wea_windrose.pl?nvprca.]
Wielicki, B. A., B. R. Barkstrom, E. F. Harrison, R. B. Lee III, S. G. Louis, and J. E. Cooper (1996), Clouds and the Earth's Radiant Energy System (CERES): An Earth observing system experiment, *Bull. Am. Meteorol. Soc.*, *77*, 853–868, doi:10.1175/1520-0477(1996)077<0853:CATERE>2.0.CO;2.
Wilkinson, J. M., A. N. Porson, F. J. Bornemann, M. Weeks, P. R. Field, and A. P. Lock (2013), Improved microphysical parametrization of drizzle and fog for operational forecasting using the Met Office Unified Model, *Q. J. R. Meteorol. Soc.*, *139*(671), 488–500, doi:10.1002/qj.1975.
Williams, A. P., R. E. Schwartz, S. Iacobellis, R. Seager, B. I. Cook, C. J. Still, G. Husak, and J. Michaelsen (2015), Urbanization causes increased cloud base height and decreased fog in coastal Southern California, *Geophys. Res. Lett.*, *42*, 1527–1536, doi:10.1002/2015GL063266.
Wood, R. (2012), Stratocumulus clouds, *Mon. Weather Rev.*, *140*(8), 2373–2423, doi:10.1175/mwr-d-11-00121.1.
Wood, R., and C. S. Bretherton (2006), On the relationship between stratiform low cloud cover and lower-tropospheric stability, *J. Clim.*, *19*, 6425–6432, doi:10.1175/jcli3988.1.
Yin, J. F., D. H. Wang, G. Q. Zhai, and H. B. Xu (2014), An investigation into the relationship between liquid water content and cloud number concentration in the stratiform clouds over north China, *Atmos. Res.*, *139*, 137–143, doi:10.1016/j.atmosres.2013.12.004.